Bird detection algorithm for the WSR-88D radars

Report on ROC MOU-2018 task 14.

Precious Jatau[1,2] and Valery Melnikov[1,3]

[1] University of Oklahoma, Cooperative Institute for Mesoscale Meteorological Studies, Norman, Ok.

[2] University of Oklahoma, Advanced Radar Research Center, Norman, Ok.

[3] NOAA/OAR National Severe Storms Laboratory, Norman, OK.

28 September 2018

Contents

1. Introduction

Weather radars are designed to monitor severe weather and measure precipitation. The USA network of WSR-88D (Weather Surveillance Radar - 1988 Doppler) consists of 160 systems deployed across the continental US, Alaska, and in Puerto Rico. Sensitivity of the radars are sufficient to observe echoes from insects, birds, and bats. The WSR-88D classify such echoes as biological scatters without distinguishing the taxa. Distinguishing radar echoes from birds and insects is important for weather observations, aviation, ecology, agriculture, and biology.

Bird strikes are a major hazard for aviation. They are defined by the Federal Aviation Administration (FAA) as collisions between a bird and an aircraft resulting in the injury/death of the bird, damage of the aircraft or both. (Seidenman and Spanovich 2016). Perhaps the most high-profile incident occurred on 15 January 2009. The US Airways Flight 1549 encountered a flock of Canada Geese shortly after takeoff from the New York City LaGuardia Airport. Some birds were ingested into both engines leading to loss of thrust. Luckily, the pilots successfully landed the airplane on the Hudson River (Fig. 1.1) saving the lives of all 155 people on board.

Fig. 1.1, Hudson landing of flight 1549 caused by engine shut down due to bird strike (Source: CNN)

Many bird strikes have caused deaths and damage of aircraft. According to the National Wildlife Strike Database (Federal Aviation Administration, 2016), the number of reported annual strikes has increased 7.4 times from 1,847 in 1990 to a record 13,795 in 2015. Within this timeframe, 169,856 strikes were reported either as happened in the USA or by U.S

registered aircraft in foreign countries. Birds accounted for 95.8 percent of the 2015 reported strikes. Table 1 presents the number of bird strikes reported by the U.S airports in 2011 – 2014.

Table 1. Bird strikes reported by US airports between 2011 – 2014 (Seidenman and Spanovich 2016).

The Top 10 U.S. Airports for Reported Bird Strikes, 2011-14

Denver Intl. Airport	1,830
Dallas/Fort Worth Intl. Airport	1,482
Chicago O'Hare Intl. Airport	982
Philadelphia Intl. Airport	844
John F. Kennedy Intl. Airport	829
Salt Lake City Intl. Airport	762
Memphis Intl. Airport	746
Orlando Intl. Airport	666
LaGuardia Airport	616
Total Reported Globally	**65,139**

Although, there is a substantial risk of aircraft bird strike being to the windshield, nose, wing/rotor and radome, the engines sustained the highest percentage of damage of major components. Fig 1.2 and 1.3 below show bird damaged aircraft cockpit and engine. The FAA reports that in 1990-2015, there were 16,636 cases of bird strikes on engines of which 27 percent resulted in damage. About 5 percent of damaged engines required removal (Seidenman and Spanovich 2016). Globally wildlife strikes have killed more than 262 people and destroyed over 247 aircraft since 1988. The annual cost of wildlife strikes to the USA aviation industry in 2015 is estimated to be at least $229 million in direct and other monetary losses.

Fig. 1.2 Damaged aircraft cockpit by bird strikes. (Patterson 2016; Seidenman and Spanovich 2016).

Fig. 1.3 Damaged aircraft engine by a bird strike (Wikipedia, 2009).

The trend of bird strikes is expected to increase because of a growth in the population of large birds and increasing air traffic. Out of 30 species of birds found to frequently strike aircraft, it was found for every 100g increase in body mass, there was a 1.26% increase in the likelihood of damage. As such large birds like geese, pelicans, cranes and eagles are especially dangerous. Several methods currently exist for wildlife management around airports. They include avian radars (US FAA Advisory Circular 2010, Bunch and Herricks 2010, Nohara et al. 2011), habitat management, technology for deterring wild life species, sound systems to keep birds away from take-off/landing areas, satellite telemetry and other animal tracking techniques. Mounted lighting systems are also used to illuminate aircrafts so that incoming birds can easily detect and avoid them. While all these methods are effective for tracking/repelling birds, they do not provide the continental scale continuous surveillance of the WSR-88D network. An algorithm for detecting birds using the WSR-88D would improve aviation safety. As such, the main goal of this report is to develop an algorithm that detects the presence of birds in the terminal region of an airport.

Distinguishing birds and insects is also important for meteorology, agriculture and biology. Insects are perfect wind tracers because of their lower mass and passive flight. Birds on the other hand have a heavier mass and are active fliers. They have been found to bias wind measurements with their flight velocities (e.g., Wilczak et al. 1995, Jiang et al. 2013). Identifying radar echoes from insects and birds can improve the accuracy of radar derived winds. Furthermore, many insect species are agricultural pests. They feed on plants reducing the yield. Integrated pest management (IPM) techniques seeks to address this problem, by ascertaining the presence, abundance and distribution of these insects before taking environmentally sensitive measures to reduce the insect population (Zehnder 2014). Ornithologist also study radar patterns to understand large scale bird behavior.

The WSR-88D is a very sensitive system. It can detect a small single bird at distances up to 100 km from radar. Most probable times of bird strikes are periods of bird migration. Birds migrate intensely at fair weather, which is called “clear air” in radar meteorology. In “clear air” situations, no precipitation is observed, but radar can show large echoes from birds, bats, and insects, which is called atmospheric biota. Birds typically migrate at night when there can be some nocturnal insects. In the day time, some birds forage on insects. Birds and insects should be expected to be found at any time of the day. They also produce similar radar echoes creating the challenge of knowing exactly what taxa is being observed. Many clear air studies are based on reflectivity which is highly variable depending on radar cross section and abundance of scatterers in the atmosphere. Current radar algorithms like The Hydrometeor Classification Algorithm used on the WSR-88D network defines a broad biological class of echoes (Park, 2008), without identifying the taxa.

This report contains results on distinguishing two classes of biological echoes: birds and insects. The report is organized as follows. The next section presents an analysis of the properties of clear air radar echoes. Section 3 contains results necessary for a fuzzy logic algorithm to distinguish echoes from birds and insects. The algorithm is described in section 4 which also contains results on testing the algorithm. Conclusions are reported in section 5.

2. Origin of clear air echoes

The existing body of research identifies three main causes of clear air return: birds (e.g., Eastwood 1967, Gauthreaux et al. 1998, Chilson et al. 2012, Melnikov et al. 2012), insects (e.g., Drake and Reynolds 2012) and turbulent Bragg scatter (Melnikov et al. 2011, 2013, 2017). Smoke and dust particles have been found to occasionally contribute to clear air return (Melnikov et al. 2008, 2019). Birds are large targets capable of independent flight with air speeds of 10-20 m/s (Martin 2003). Their velocities pose an issue for radar derived wind estimation at night. The NOAA’s wind profile routinely flags nocturnal clear air data as being contaminated by birds (Eastwood 1967, O'Bannon 1995, Gauthreaux and Belser 1998, Zrnic and Ryzhkov 1998, Jungbluth et al. 1995). Insects are smaller than birds and are generally wind borne except in cases of alignment where the aligned group generates its own velocity (Riley 1975). As such they are good tracers of the wind. Insects can be found at any time of the day.

Clear air reflectivity (Z) has a unique daily cycle. Martin (2003) analyzed clear air data from the Cimarron radar in May 1999. The results showed that Z had stronger nocturnal return than day time return with the lowest values recorded at sunrise and sunset. During day time, Z maintained a modest value concentrated at a low height. This continued till sunset at 2 UTC where it reaches the first minima. In the next 1 hour, Z rapidly increases to its maximum value contained a greater height (2 - 3 km). The average nocturnal value remained high between 4 – 10 UTC after which it rapidly dropped to the second minima at sunrise (11 UTC) followed by a quick increase to around initial day time Z values. This cycle implies a clear change in nature (probably taxa) of scatterers between day and night. Hardy and Glover (1966) suggested that the daily cycle is due to insect of one specie leaving and another

ascending. However, results from the analysis of dual pol variables in this research, show that the more plausible explanation is more insects flying during the day and birds dominating night returns. This is also supported by other research.

Clear air echoes can occur as isolated targets and is often granular. Browning and Atlas (1966) discovered that nocturnal echoes have larger grains indicative of larger particulates compared to day time. This is probably due to more birds being aloft. Clear air echoes can also occur as layers or volumes (Martin 2003, Martin and Shapiro 2007). Furthermore, clear air Z fluctuates with seasons. Generally, it is stronger in the warm season. On the Great Plains, late spring has the strongest Z at night with daily values fluctuating by as much as 20 dBZ (Martin 2003, Martin and Shapiro 2007). This correlates with the peak migrating season for birds.

Thin lines of clear air Z are a common feature of day echoes on the Great Plains. They are clearest (thinnest and sharpest) in the late afternoon. Wilson et al.(1994) attributed it to insects gathering at meteorological boundaries. Boundaries are also locations of large and sharp index of refraction gradients. Geerts and Miao (2005) studied vertical flight of scatterers in the convective boundary layer using profiling airborne radar. They found insect plumes to be collocated with updrafts. Micro-insects were also observed to resist updraft with an average speed of 0.5±0.2 m/s.

Perhaps the strongest evidence of birds are the expanding rings of reflectivity often seen at certain morning times of the year. Elder (1957) initially postulated gravity waves as the cause. However, recent research has proven that it is due to birds leaving their nesting sites evidenced by these rings always emanating from the same location (Battan, 1973, Eastwood 1967, Gauthreaux and Belser 1998). Similar rings are seen in the evening due to bats leaving their roosting sites. Other rings of 1 to 3 km diameters, which do not expand, have also observed (Martin 2003). They are attributed to convective cells (Doviak and Zrnic 1993).

PPI scans of Z for day and night frequently show bilateral symmetry with the strongest values 180 degrees apart. This also extends to dual polarization variables (Zrnic and Ryzhkov 1999). The symmetry is due to the radar cross section of a non-spherical object aligned in the atmosphere. Schaefer (1976) attributed it to aligned birds and Gauthreaux and Belser (1998) attributed it to aligned insects. Insects aligned in the atmosphere can also produce asymmetric radar echoes (Melnikov et al. 2015).

2.1. Nocturnal clear air echoes

Migratory birds have been found to travel mostly at night, sometimes in flocks but also individually. Thus, nocturnal echoes in bird migration seasons are dominated by birds. NOAA's Enviromental Technology Lab considers this a severe problem and routinely the flag low level radar wind profiler data, collected at night during migration season as bird contaminated (van de Kamp et al. 1997, Miller et al. 1997, Wilczak et al. 1995). This was further corroborated by differences in balloon sounding data and radar derived winds during

certain periods of the year at night time where birds are expected to migrate. O'Bannon (1995) and Gauthreaux et al. (1998b) report on this issue with the WSR-88D VAD wind profiles. The differences recorded were as large as 15 m/s which is consistent with the expected velocities for birds.

While many birds are expected in nocturnal echoes during a migration season, it does not exclude other sources like insects. Gossard and Strauch (1983) counted separate echoes with a 1.5 m resolution FM-CW radar on a night in July in Nebraska. They found a density of 1 echo per 12 meter cube over a depth of 500m. Martin (2003) concluded that this density would imply about 46 billion species over the state of Oklahoma alone which certainly excludes birds as the only cause of nocturnal echoes. Furthermore, birds have been observed to have reflectivity in the range of 5 to 15 dBZ (Gauthreaux and Belser 1998). One bird in a radar probe volume can account for 10 dBZ of echo (O'Bannon 1995). Martin (2003) estimated that using a probe volume of 100-meter cube and 1 bird per volume over the state of Oklahoma through a depth of 3 km will require 500 million birds at the instant of a radar scan which is highly improbable. Other scatterers (probably insects) must be present in nocturnal echoes to explain this number.

2.2. Day time clear air echoes

Most day time echoes are caused by insects. They are usually spread over a wide area and more uniformly distributed than birds in the atmosphere. Crawford et al. (1949) concluded that insects are the cause of nearly all day time clear air echoes. This was based on the difficulty in creating gradients in refractive index strong enough to be sensed by the radar and visual confirmation of the presence of insects coinciding with radar observations.

Many other studies by entomologists have also confirmed insect dominance of day time clear air echoes. Drake (1984, 1985) studied moths in a nocturnal low-level jet in Australia. He observed bilateral symmetry in Z due to alignment of scatterers using a 3.2 cm wavelength radar. Rapid increase in reflectivity at dusk was observed and attributed to mass insect takeoff. Aerial trappings with a kite borne net confirmed the presence of moths up to 220 m. Drake (1984,1985) also reported radar cross section values of 1 cm^2 typical of large insects. These observations led to the belief that measured echoes were from insects.

Hardy and Katz (1969) compared clear air Z using radars with wavelengths of 3, 11 and 71 cm. They discovered that reflectivity of dot echoes in the lower troposphere decreased at higher wavelengths, consistent with Rayleigh scattering off objects smaller than radar wavelength. Wilson et al. (1994) also used multiple radars with different wavelengths to study clear air echoes and concluded that insects were the cause of day echoes.

Kropfli (1986) used 3.22 cm and 0.86 cm radars to study the convective boundary layer during the day. They found difference between VAD winds and wind measured with a tall anemometer of about 0.2 m/s indicative of wind borne scatterers. Furthermore, typical clear air Z of -15 to 5 dBZ are much higher than expected from the returns due to index of

refraction gradients. They also noted an absence of maximum Z near inversion heights, ruling out refractive index gradients as the source. Based on these observations, Kropfli (1986) concluded that day clear air return was due to insects, seeds and particulates in the atmosphere. The WSR-88D is capable of observing thermal plumes partially filled with insects (Melnikov and Zrnic 2017). Hardy and Katz (1969) reported the presence of Bernard - like cells seen during the day at the same time an abnormal number of airborne ants were observed. However, it should be noted that birds can migrate any time of the year.

2.3. Classifying birds vs insects

Most studies by meteorologists, ornithologists, and entomologists use few variables to identify clear air echoes. However this approach will is error prone because NEXRAD variables are sensitive to target properties like location, range, aspect and radar cross section. For example, reflectivity depends on both radar cross section and abundance of scatterers in a range gate. Birds should generally have a higher average radar cross section. However, their backscatter cross section is in the resonance region. Some insects also have resonant cross sections. This means that a large insect observed broadside and a small bird observed head on can have similar cross sections. Thus, their respective Z values can be difficult to differentiate. A strong Z echo can be due to a single bird, many insects, or a combination of both.

For a more robust classification, all other radar variables should be used. Birds are known to have higher velocities than insects. Consequently, radial velocities of birds will also be larger. Bachmann and Zrnic (2006) analyzed the power spectrum of a resolution volume located in the wind direction. They found two peaks in the spectrum around 12 m/s and 20 m/s which they attributed to birds and insects respectively. Spectrum Velocity Azimuth Displays (SVAD) also showed insects with a differential reflectivity (ZDR) maximum between 3 and 8 dB while birds have a $ZDR < 2.5$ dB. Insects generally have higher ZDR than birds.

Furthermore, birds engage in more wind independent flight than insects. As such, resolution volumes dominated by birds would have a higher variation of radial velocities (σ_V). Similarly, birds are less coordinated and uniformly distributed than insects when flying and should have a lower correlation between horizontal and vertical polarizations ρ_{HV}. Finally, birds have more liquid content than insects. Birds frequently exhibit higher differential phase (ϕ_{DP}) values than insects (Zrnic and Rhyzkov 1998).

More information can be derived from the WSR-88D's level II products. A texture of these products is calculated as the spatial variability over a 3-range gate by 3-range gate contiguous volume (or texture volume) to obtain 6 products. They reveal patterns of clear air echoes that might exist over a larger spatial scale.

3. Introduction to the algorithm

Radar data from WSR-88D KTLX radar located in central Oklahoma were analyzed. Previous examination of radar data shows that Z from birds and insects can have close values. Therefore, a simple reflectivity threshold cannot be used alone to distinguish these scatterers. Other properties of the base data or/and dual – polarization (dual pol) radar parameters need to be utilized. The base data include Z, Doppler velocity V, and spectrum width σ_V. The dual polarization parameters are ZDR, φ_{DP}, and ρ_{HV}. The texture of a radar variable provides information about its spatial variability. The texture of each radar variable is also analyzed for potential information on separating echoes from birds and insects.

The algorithm will be applicable between 10 to 100 km from the radar. This is sufficient range for the terminal airport area, which typically has a radius of 50-70 km around an airport. Range gates that are located at less than 10 km from the radar are not considered because measurements are contaminated by ground clutter. Radar data show that all radar parameters vary with the distance from radar and azimuth of the radar beam. Therefore, the algorithm should have variable parameters which depend on the distance from radar. The following distance intervals are chosen for the algorithm: 10 – 20, 20 - 30, 30 – 40, 40 – 50, 50 - 60, 60 - 70, 70 - 80, 80 – 90, and 90 – 100 km. These are 9 range intervals. The radar parameters inside the intervals will be averaged to reduce natural fluctuations of the radar estimates.

3.1. Selection of clear air days

To obtain radar parameters for the algorithm and to tune it, cases with dominant reflections from insects and birds are needed. It is known that September is a month with intense nocturnal bird migration in Oklahoma, so it is chosen as the bird migration case. Clear air days, i.e days without precipitation were obtained from the Norman station of the Oklahoma Mesonet (Fig 3.1). All days with rainfall less than 0.1 inches are selected. They are September 1,3-16 and 19 -25 all in 2017. This is a total of 22 clear air days.

Radar data were collected in two resolutions: standard and super resolutions. In the standard resolution, azimuthal sampling is done every 1 azimuthal degree for a total of 360 radials per elevation. For the super resolution, azimuthal sampling is done every 0.5 degree (720 radials per elevation). It is normally used for the lowest 2 or 3 elevation scans. KTLX switches between clear air and precipitation operating modes: these modes are chosen by comparing areas of currently measured reflectivity from precipitation to a predefined area threshold. Each mode contains different Volume Coverage Patterns (VCP) to maximize volume coverage. Clear air mode utilizes VCPs 31 and 32.

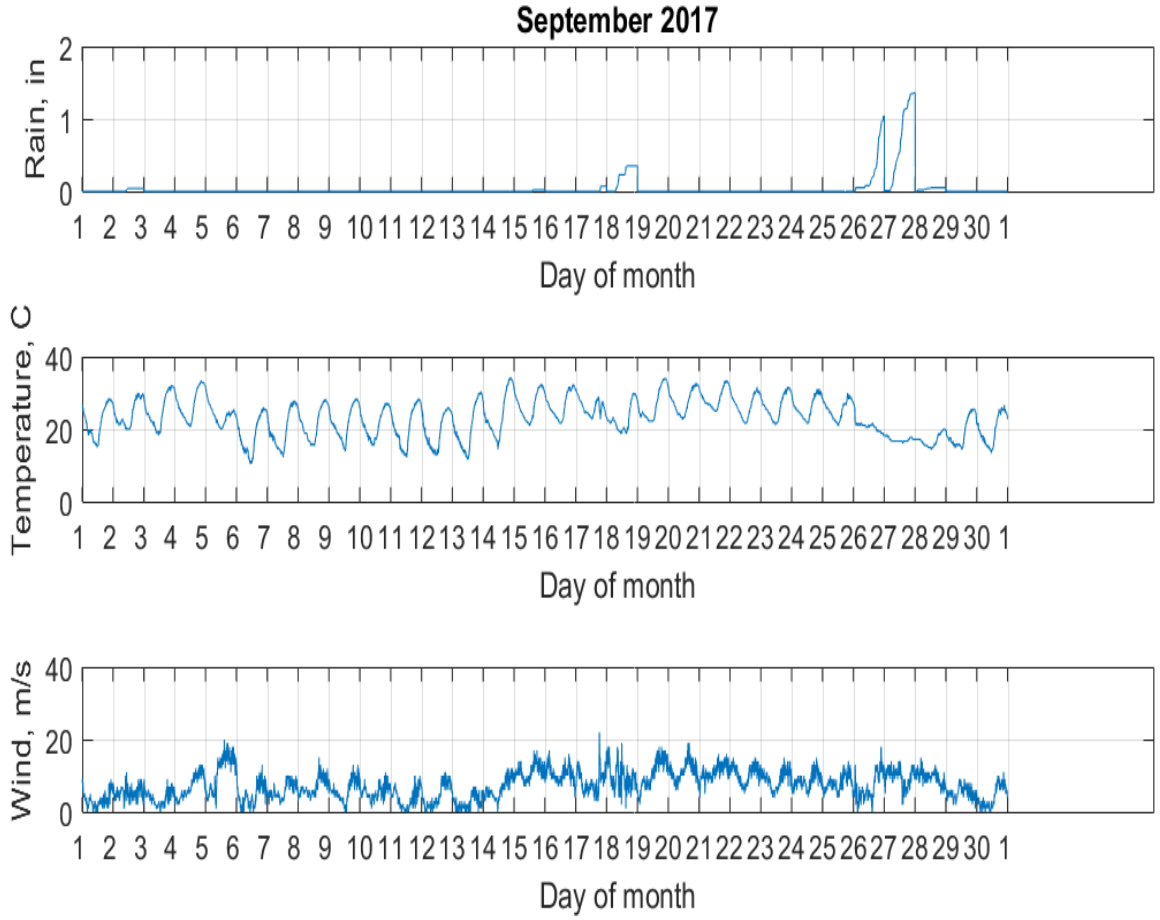

Fig. 3.1. Oklahoma Mesonet sounding for September 2017, the Norman station.

Data were combined from the two lowest elevation sweeps. The lowest elevation (Surveillance sweep) contains all dual polarization variables and Z for ranges up to 460 km while the next elevation sweep (Doppler) contains Z, V and σ_V. Since both cuts are separated by less than a minute, they are considered as one sweep. The Z estimate from the Doppler sweep is chosen because it uses more radar pulses which translates to higher accuracy while maintaining a maximum unambiguous range of 148 km. This range is sufficient for the requirements of this study. Figure 3.2 and 3.3 show fields of radar variables for the clear air scans, 4 Sept, 2017 at 20:00 UTC and midnight on 5 Sept, 2017. The field order in the figures are Z, V, σ_V, ZDR, φ_{DP} and ρ_{HV}.

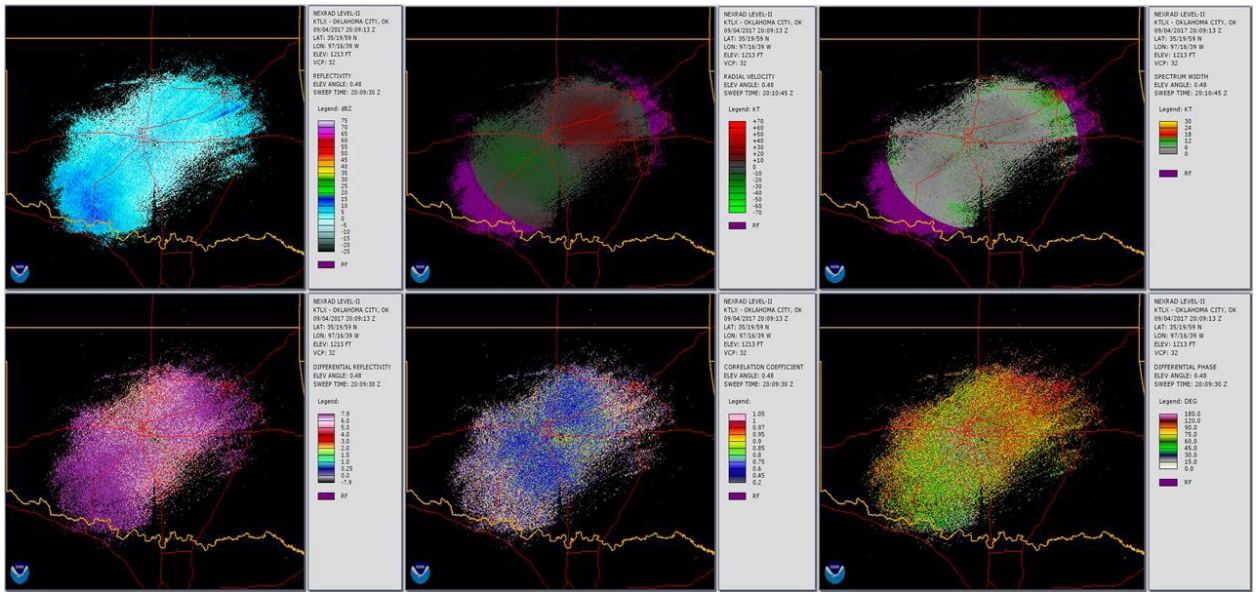

Fig. 3.2. PPI from Day Time (20:00 UTC). WSR-88 D KTLX, 4 Sept, 2017.

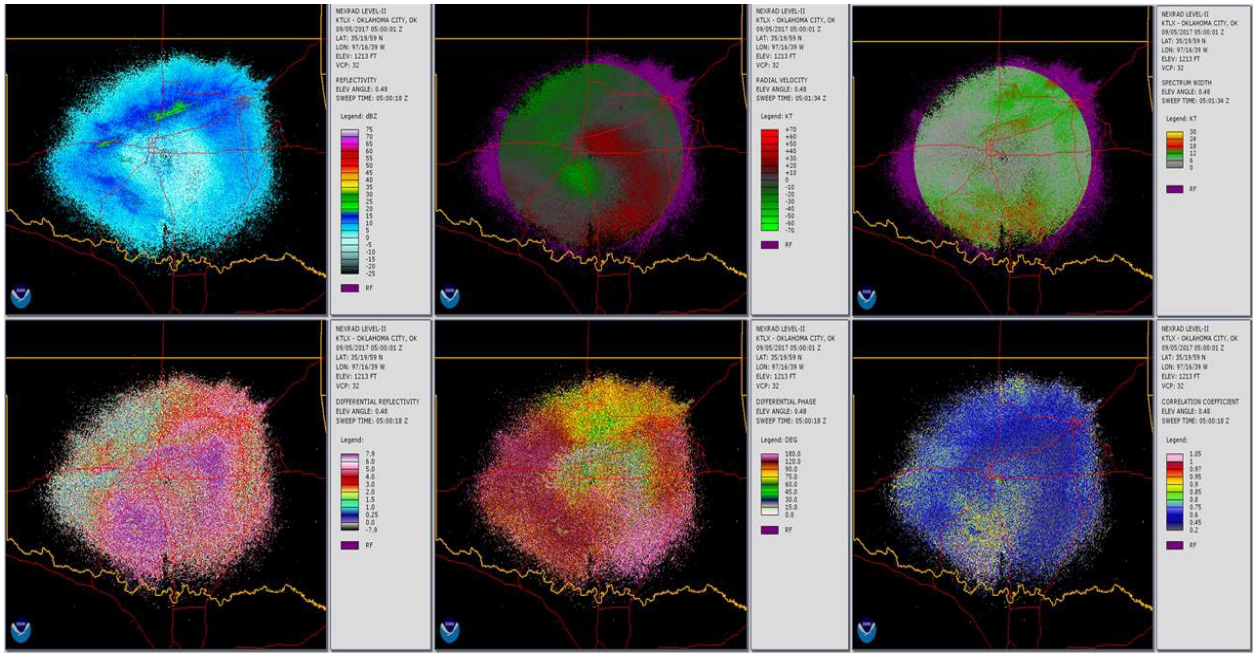

Fig. 3.3. Same as Fig 3.2 but for Midnight 5th Sept, 2017.

3.2. Data processing

The distributions of radar parameters for birds and insects have to be obtained for the algorithm. Previous studies have shown that during migratory season, birds dominate night time clear air echoes while insects dominate day time clear air echoes. In this study, day time is defined as 14 - 21 UTC (9 – 16 CDT) while night time is defined as 2 - 9 UTC (21 – 4 CDT). A flow chart of the data processing is shown in Fig. 3.4. The first step is to load data

from all Plan Position Indicators (PPIs). Next, data quality control (or data preprocessing) is applied to remove data points that have either a low Signal to Noise Ratio (SNR), no measured values, precipitation or ground clutter. The third step is to calculate the texture of all radar variables. In the final data processing step, radar data is averaged first over 10 km along the radials and then each 10 km pixel is averaged over 30 minutes. The result of this step is 6 Median of Median Textures (MOM) and 6 Mean of Mean (MM) variables, totaling 12 parameters. Sections 3.2.1 – 3.2.3 presents more detail on data quality control, texture and data processing.

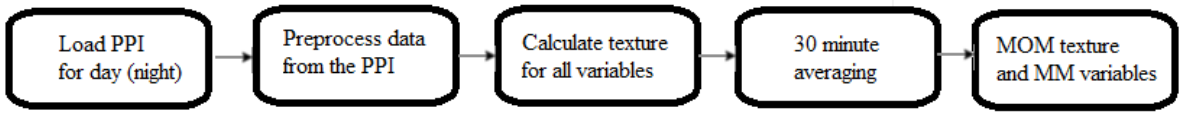

Fig. 3.4. Flow chart of the data processing algorithm

3.2.1. Data quality control

Data were analyzed in 10 km intervals from 10 to 100 km. Low SNR range gates and gates with anomalous propagation have been filtered out. The following thresholds are also applied

a) Data cells with values of -888 or -999 (low SNR) were removed,

b) Biological scatterers typically have low ρ_{HV} values with an upper limit of about 0.8 while precipitation have ρ_{HV} > 0.97 (Park et al., 2008). A threshold of ρHV= 0.8 has been chosen for this study to remove possible weather contamination while retaining biological echoes. All range gates with ρ_{HV} greater than this threshold are removed,

c) All range gates with radial velocities in the range [-1,1] m/s are also excluded to prevent possible contamination by ground clutter.

3.2.2. Texture

Texture provides information about the spatial variability of a radar variable over a texture volume made up of neighboring radar resolution volumes. The texture volume used is a 3 by 3 contiguous groups of gates centered on a reference gate. Each resolution volume is 0.93°×0.93° × 250m. Thus, the texture volume is $2.79°\times0.93°\times750m$. Fig 3.5 shows a texture volume made up of gates 0-9 and centered at reference gate 0. Gates 3, 4 and 5 belong to one radial, 1, 8 and7 to another and 2, 0 and 6 to the third radial. Rmin and Rmax are the lower and upper boundaries for a specified range interval. So, for a 10-20 km interval, Rmin = 10 km, and Rmax = 20 km.

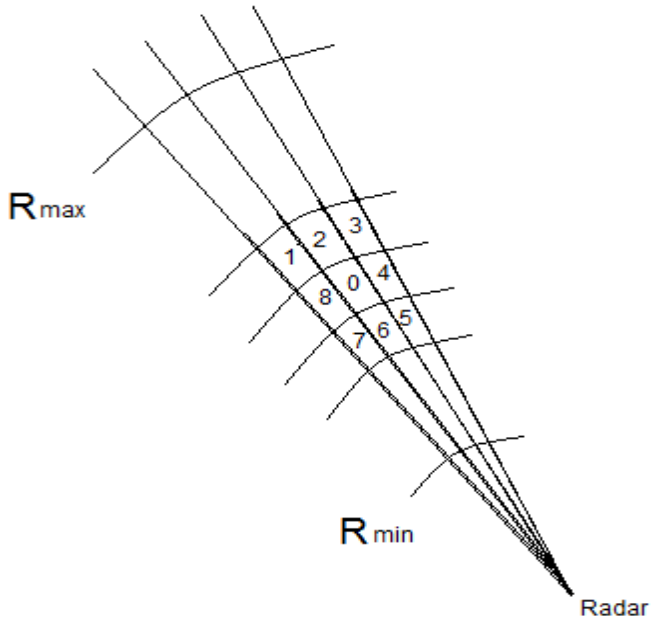

Fig. 3.5. Diagram for calculating the texture at range gate 0.

For Z, the texture $\Delta Z_{a,b}$ at radial a and range gate b is calculated as

$$\Delta Z_{a,b} = \frac{1}{N-1}\sum_{i=-1}^{1}\sum_{j=-1}^{1}\left|z_{a,b-}\, z_{a+i,b+j}\right| \qquad (3.1)$$

where i stands for the azimuthal offset and j is the range gate offset from the reference gate. N is the number of gates with measured values. Texture is only calculated if $Z_a \neq NaN$ and $5<N\leq 9$. Otherwise the texture is assigned as not available (NA). This condition ensures that the texture is always representative of at least half of the texture volume. Edge effects for the first/last radials and range gates are handled by periodic extension. Also, ΔZ and ΔZDR are calculated using the values in dB (not linear scale). The same procedure is used to obtain texture for velocity (ΔV), spectrum width ($\Delta\sigma_V$), differential reflectivity (ΔZDR), differential phase ($\Delta\varphi_{DP}$), and correlation coefficient ($\Delta\rho_{HV}$).

3.2.3. Thirty minute data processing

Data processing takes into consideration range, time and azimuthal dependence of radar variables. The goal is to process the data such that characteristics of the dominant scatterer in the radar volume are emphasized. Data are processed along each radial, in 10 km range intervals; they are also processed in 30-minute (half hour) intervals. For instance, for a radial at 20°, a half hour interval of 01:00-01:30 UTC and range interval 10-20 km, the procedures are

a) The texture of each variable is found using equation (3.1) for each PPI.

b) Median of texture along the 20° radial and between the 10 – 20 km interval is found.

c) All median textures in step b) is compiled for all PPI's within 01:00-01:30 UTC.

d) The median is found for the compiled textures in c). This statistic will be called the median of median (MOM) texture.

e) Repeat a) to d) for all radials, range intervals and time intervals.

This procedure is also used to analyze the original variables the only difference being that mean is used instead of the median, and step a) is omitted. The resulting statistic will be called the mean of mean (MM) variables

3.3. Results

This section presents the distributions of radar parameters for night and day echoes. Each data point denotes a MOM texture or MM variable. The blue histograms represent data from night echoes while the red represents data from day echoes. All 12 parameters are compared to determine which ones show good enough separation between the two taxa. The day time distributions are assumed to be from insects while night time ones are assumed to be from birds.

3.3.1. Reflectivity Z

Reflectivity shown in Fig.3.6 has a higher median for night time for all range intervals. This is expected because at night many birds are aloft in the atmosphere. Since they are bigger than insects and quite dense, they produce higher returned powers. This parameter has very good separation between distributions for bird and insect echoes.

3.3.2. Velocity V

Birds are active fliers and would produce higher velocities than insects which are wind borne. This can be seen in Fig 3.7 with night velocity between ±25 m/s while day velocities are between ±20 m/s. The wind velocity changes during a day and the Doppler velocity depends on wind velocity. The Doppler velocity also depends on the flight direction of birds/insects and is a projection of their true velocity unto the direction of the radar beam. As a result, the distributions can be seen to be poorly separated.

3.3.3. Spectrum width σ_V

Spectrum width measure the variation of velocities within the resolution volume. Bird occupied volumes will have a wider range of velocities compared to insect occupied volumes because birds are more active fliers than insects. Thus, the spectrum width for birds will be higher. This can be seen in Fig 3.8 where birds have a higher median σ_V than insects across all ranges. Both distributions are also well separated.

3.3.4. Differential reflectivity ZDR

Zrnic and Ryhzkov (1998) observed higher ZDR values (up to 10 dB) for insects compared to birds. This can be seen in Fig 3.9 where insect distributions have higher values across all ranges. Also, From 30 – 100 km, many insect values accumulate around 8 dB because this is

the highest ZDR that WSR-88D can measure. Actual values are ≥ 8 dB, consistent with the previously mentioned studies. Both distributions are also well separated.

3.3.5. Differential phase φ_{DP}

Zrnic and Rhyzkov (1998) also found that birds had higher φ_{DP}, sometimes exceeding 100° compared to insects. Median values for bird φ_{DP} (seen in Fig 3.10) can be seen to be ≥ 100° and are also greater than median value for insects across all ranges. Furthermore, φ_{DP} shows very good separation for birds and insects.

3.3.6. Correlation coefficient ρ_{HV}

Birds are large targets compared to radar wavelength, move in a less coordinated manner and are usually less uniformly distributed than insects in the radar volume. They will have a lower correlation coefficient compared to insects. This can be observed in Fig 3.11 where insects have a higher ρ_{HV} for all ranges. Even though separation between birds/insects is not very large, it is consistent. Thus the distributions are considered to be well separated.

3.3.7. Velocity texture ΔV

Velocity texture gives information about the variation of the mean Doppler velocity within texture volumes. Bird flight is less wind dependent than insect one, so it is expected that this variation is higher for bird dominated echoes. It can be seen in Fig.3.12 that median bird ΔV is higher than that of insects for all ranges. ΔV is chosen for use in the algorithm instead of V. Thus, the variation in V due to projection of actual target velocities to the radar beam direction and change in wind velocity is minimized. Distributions for ΔV are well separated.

3.3.8. Spectrum width texture $\Delta\sigma_v$

The separation between birds/insects for $\Delta\sigma_v$ (Fig 3.13) is not obvious for 10-50 km. However, at 50-100 km from the radar birds can be seen to have higher $\Delta\sigma W$. The latter is consistent with the expectation that birds will have a larger variation in velocities. Overall, both distributions show good separation.

3.3.9. Other texture parameters

Fig. 3.14 shows the distribution of ΔZ. This parameter could in theory explain observed features of clear air Z such as granularity or volume filling. For 10 – 50 km, insects have slightly higher median values than birds. However, for other ranges, the separation between the two is not clear. Figs 3.15 – 3.17 also shows the distribution for texture of ZDR, φ_{DP} and ρ_{HV}. They all have similar modes in their distribution for birds and insects thus they are poorly separated.

In summary, Z, σ_V, ZDR, φ_{DP}, ρ_{HV}, ΔV and $\Delta\sigma_v$ (7 parameters) all show good separation between distributions for birds and insects for most range intervals. Furthermore, observed features of these parameters are consistent with day echoes being insects and night echoes being birds. However, V, ΔZ, ΔZDR, $\Delta\ \varphi_{DP}$, and $\Delta\rho_{HV}$ (5 parameters) did not show clear separation.

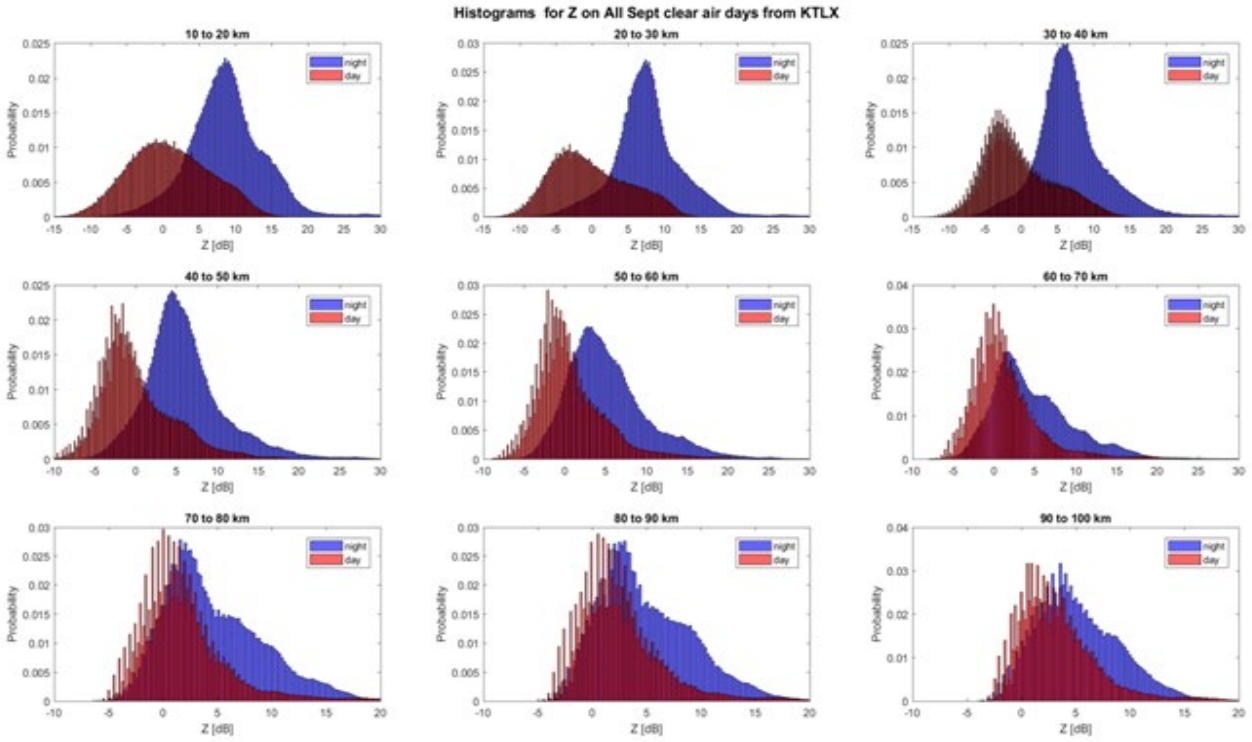

Fig. 3.6. Distribution of Z for clear air days in September 2017.

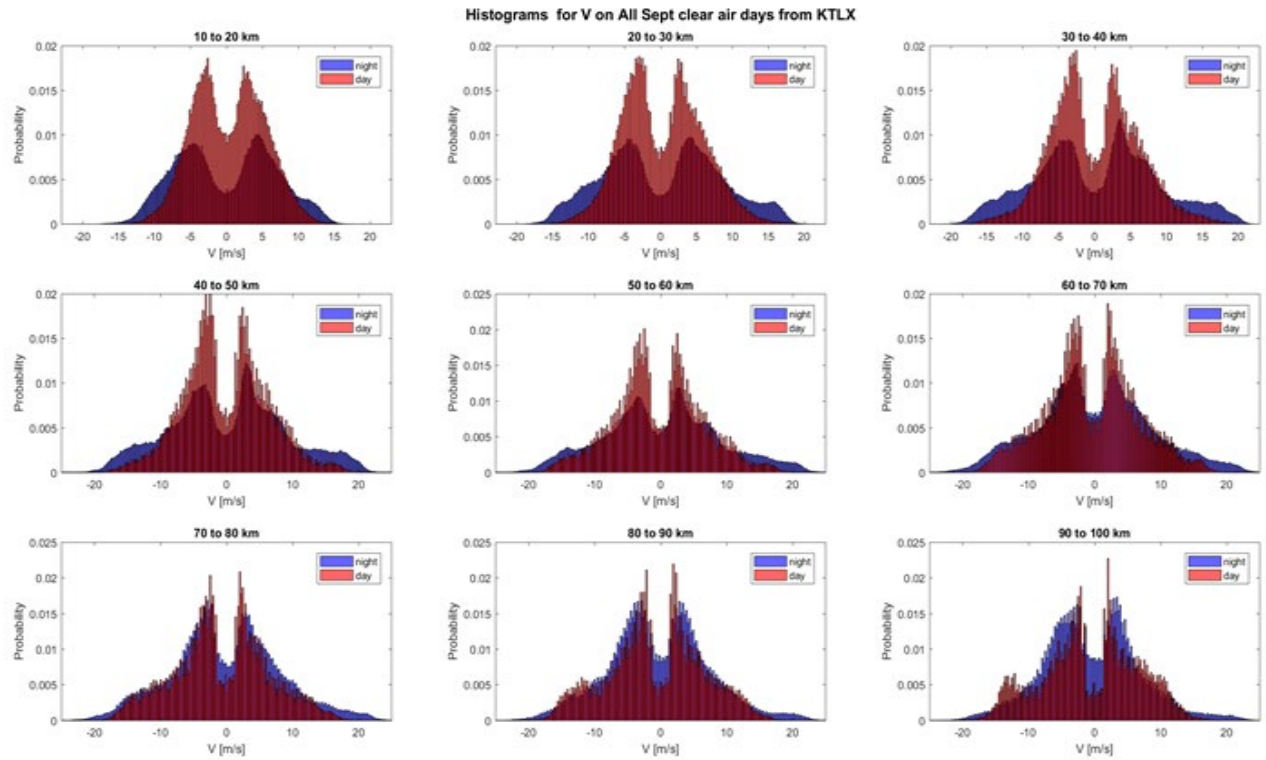

Fig. 3.7. Same as 3.6 but for *V*.

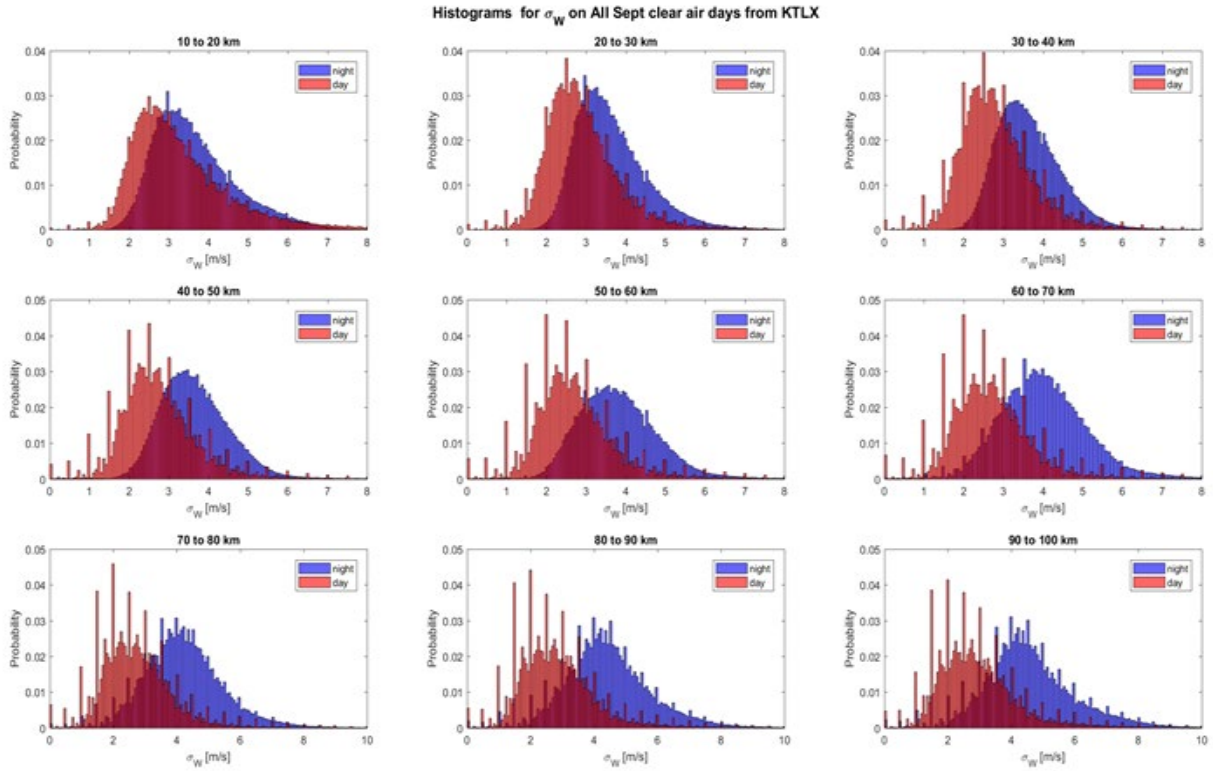

Fig. 3.8. Distribution of σ_v for clear air days in September 2017.

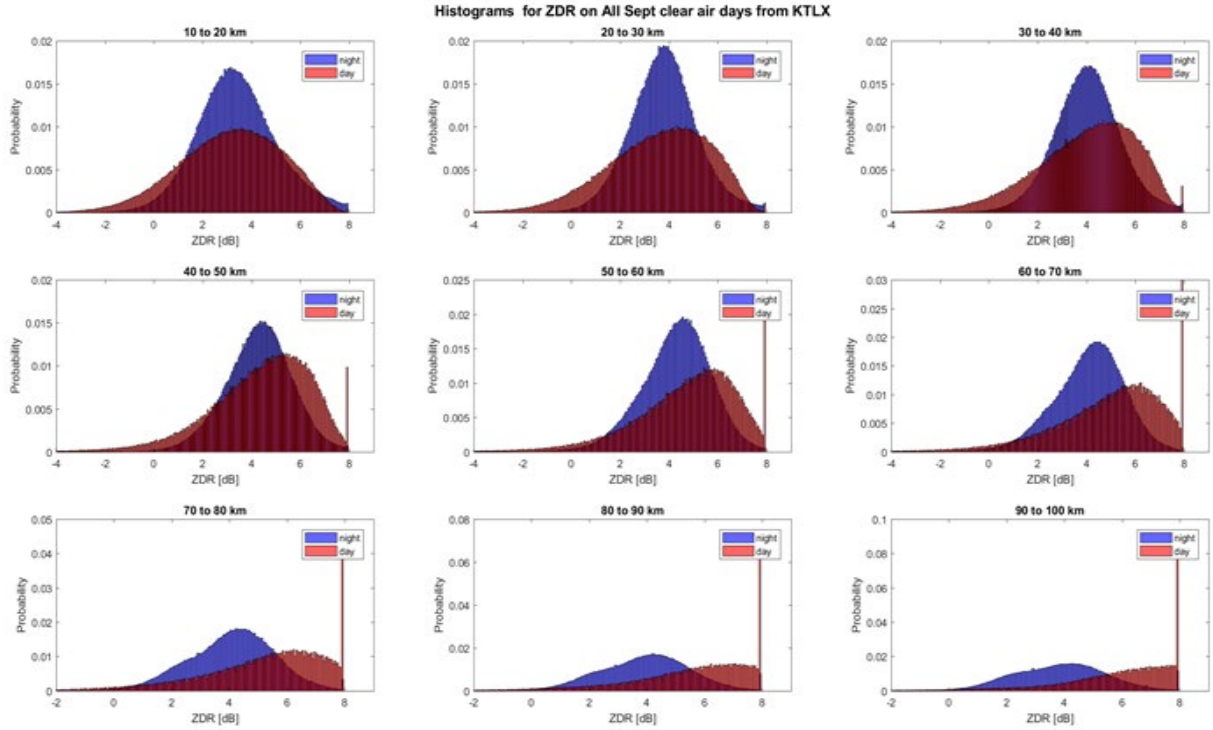

Fig. 3.9. Distribution of *ZDR* for clear air days in September 2017.

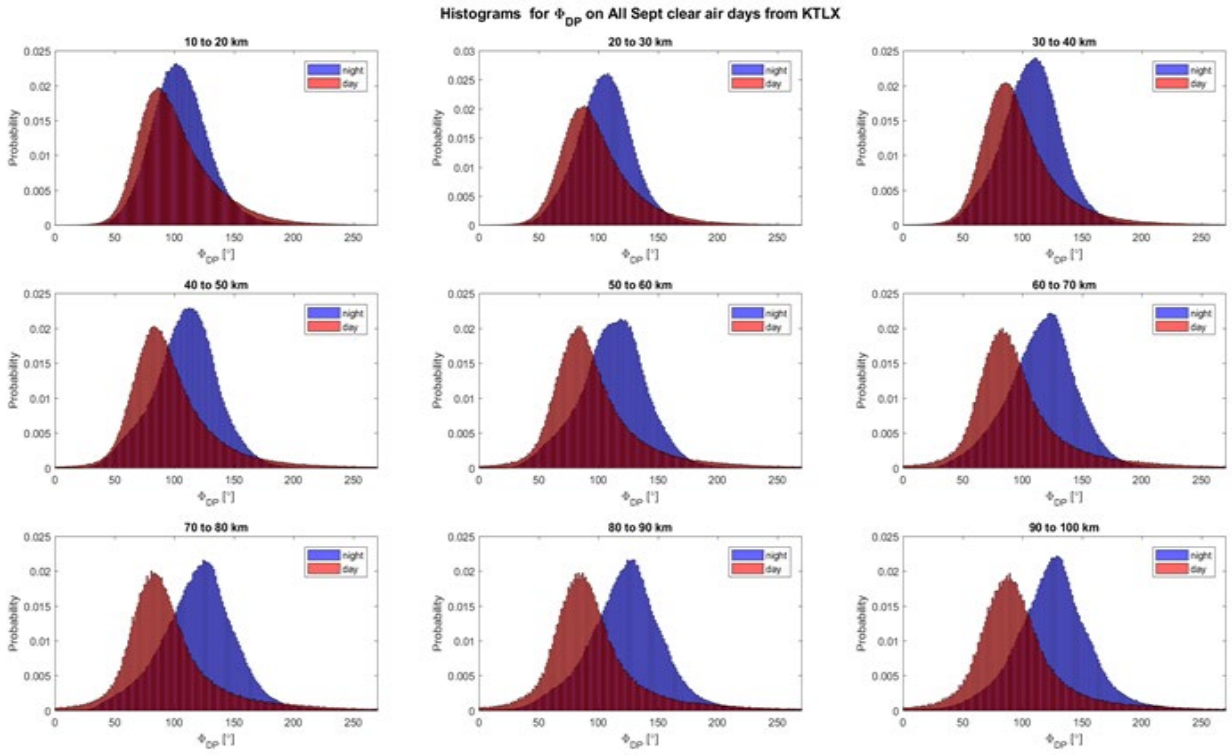

Fig. 3.10. Distribution of φ_{DP} for clear air days in September 2017.

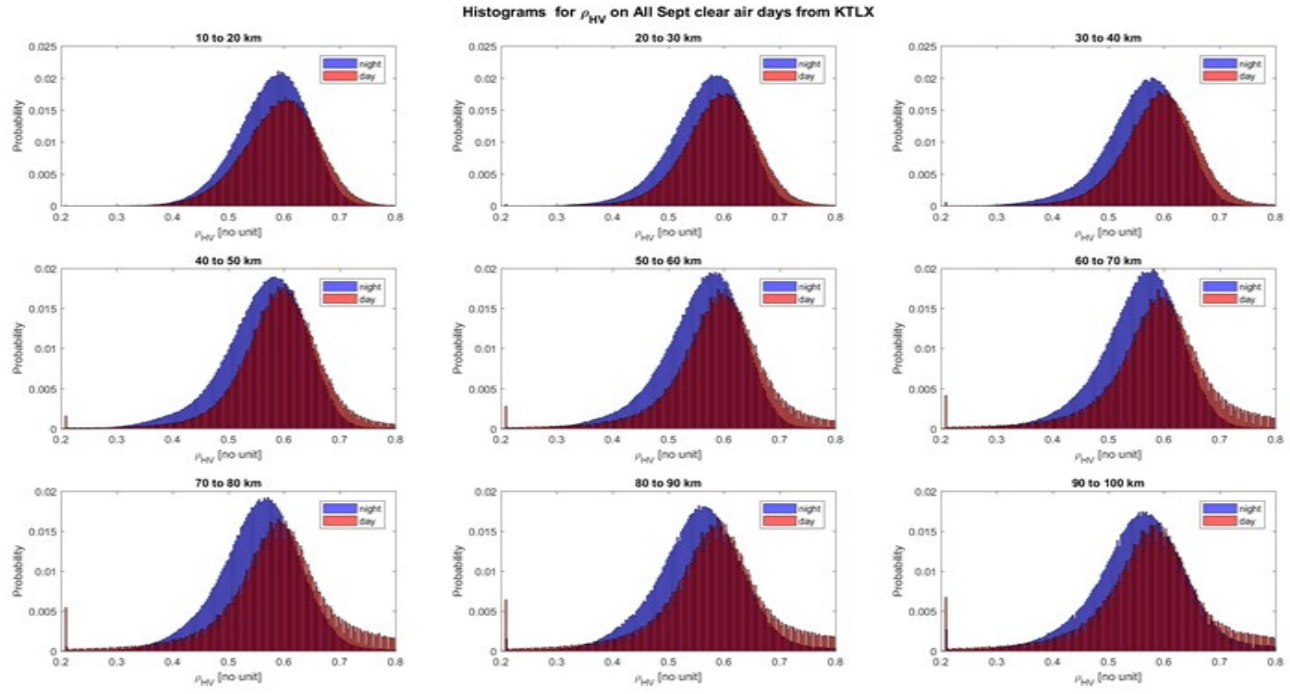

Fig. 3.11. Distribution of ρ_{HV} for clear air days in September 2017.

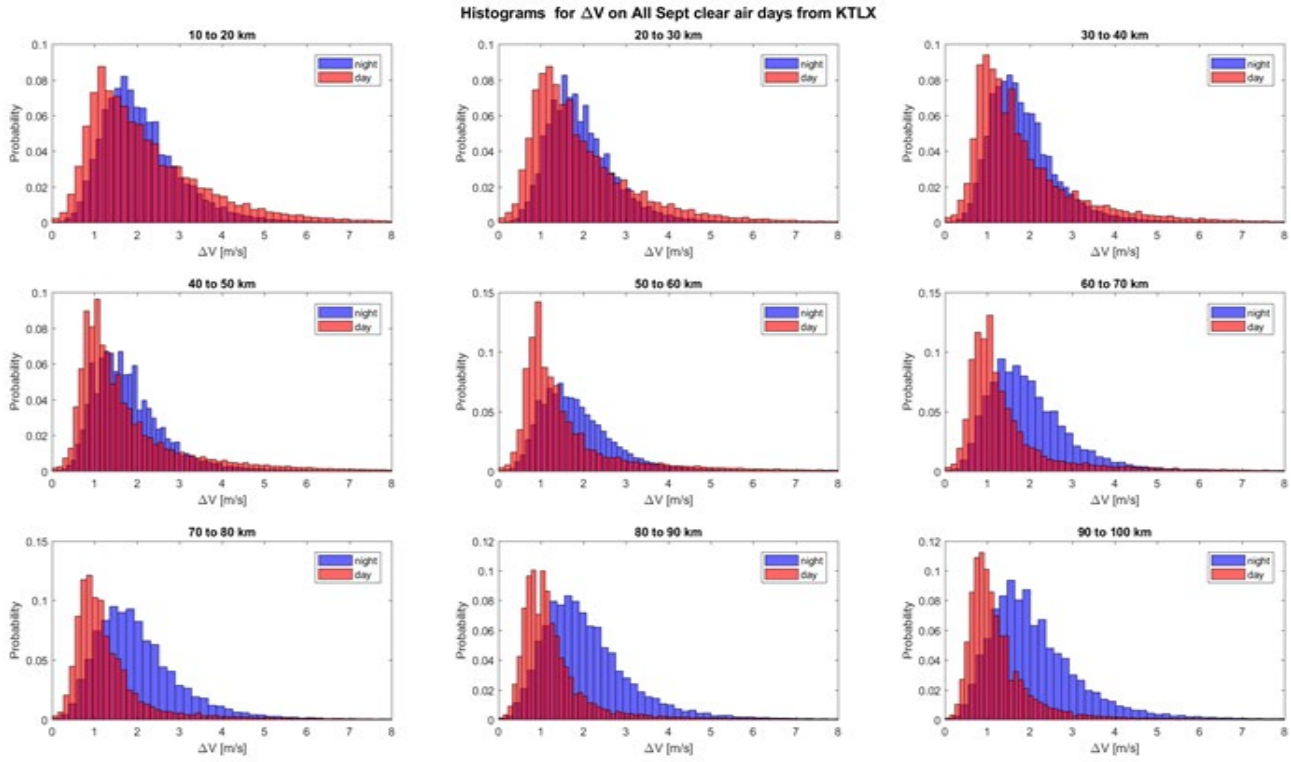

Fig. 3.12. Velocity texture ΔV.

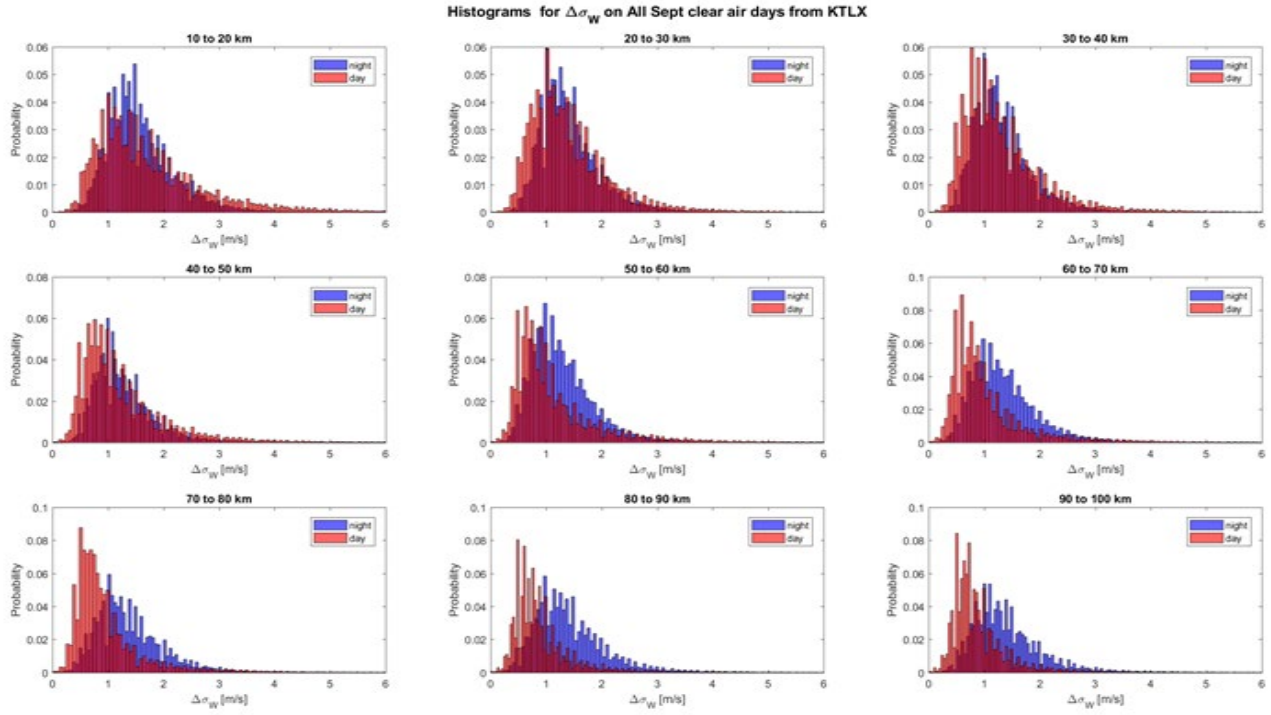

Fig. 3.13. Spectrum width texture $\Delta\sigma_v$

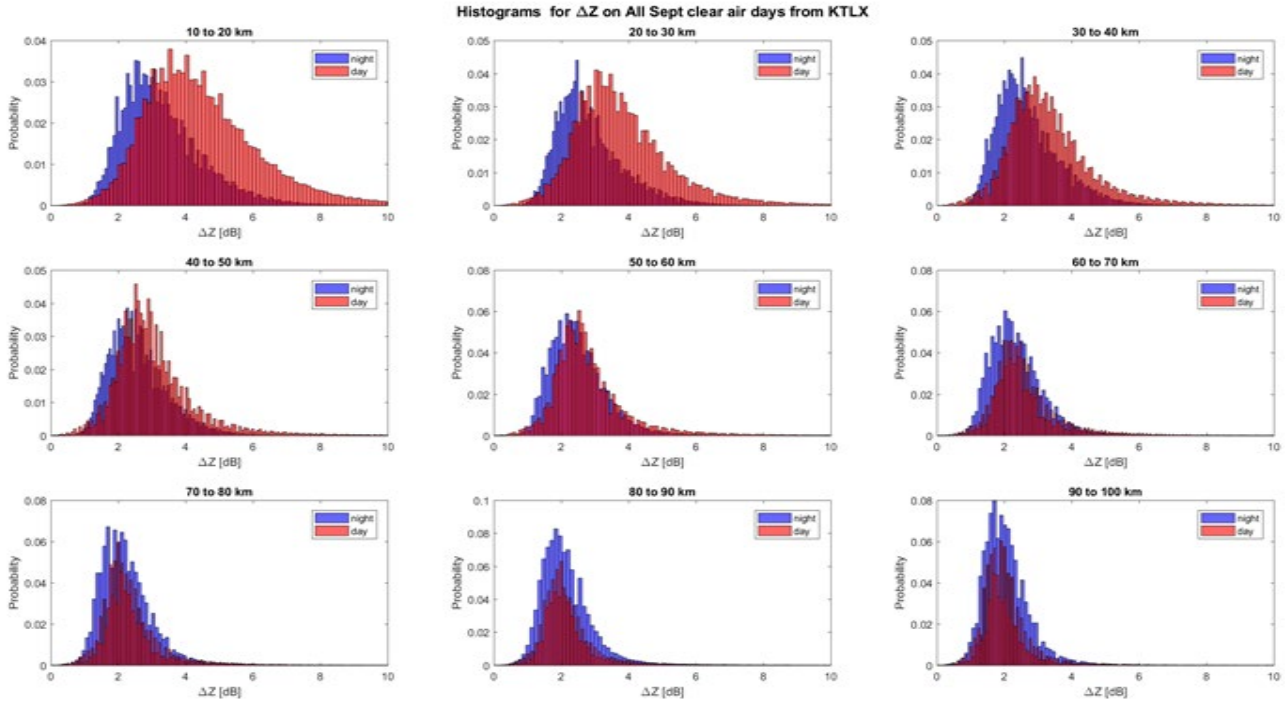

Fig. 3.14. Histogram of ΔZ for clear air days in September 2017.

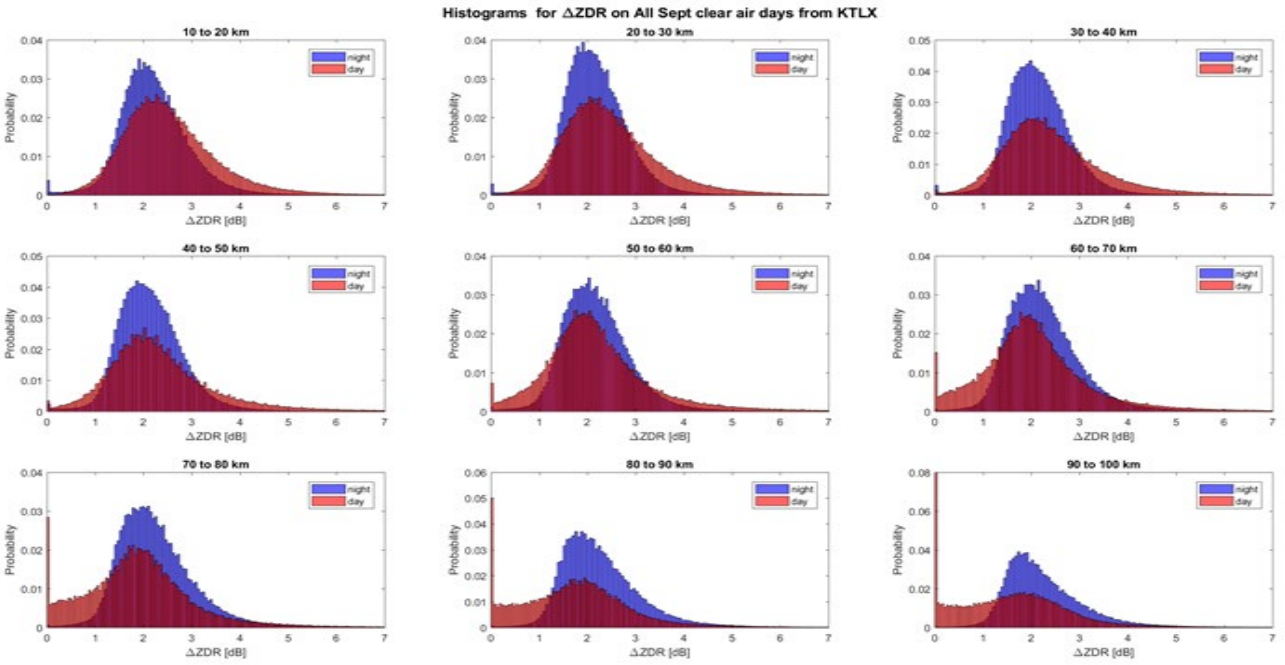

Fig. 3.15. *T*exture ΔZDR.

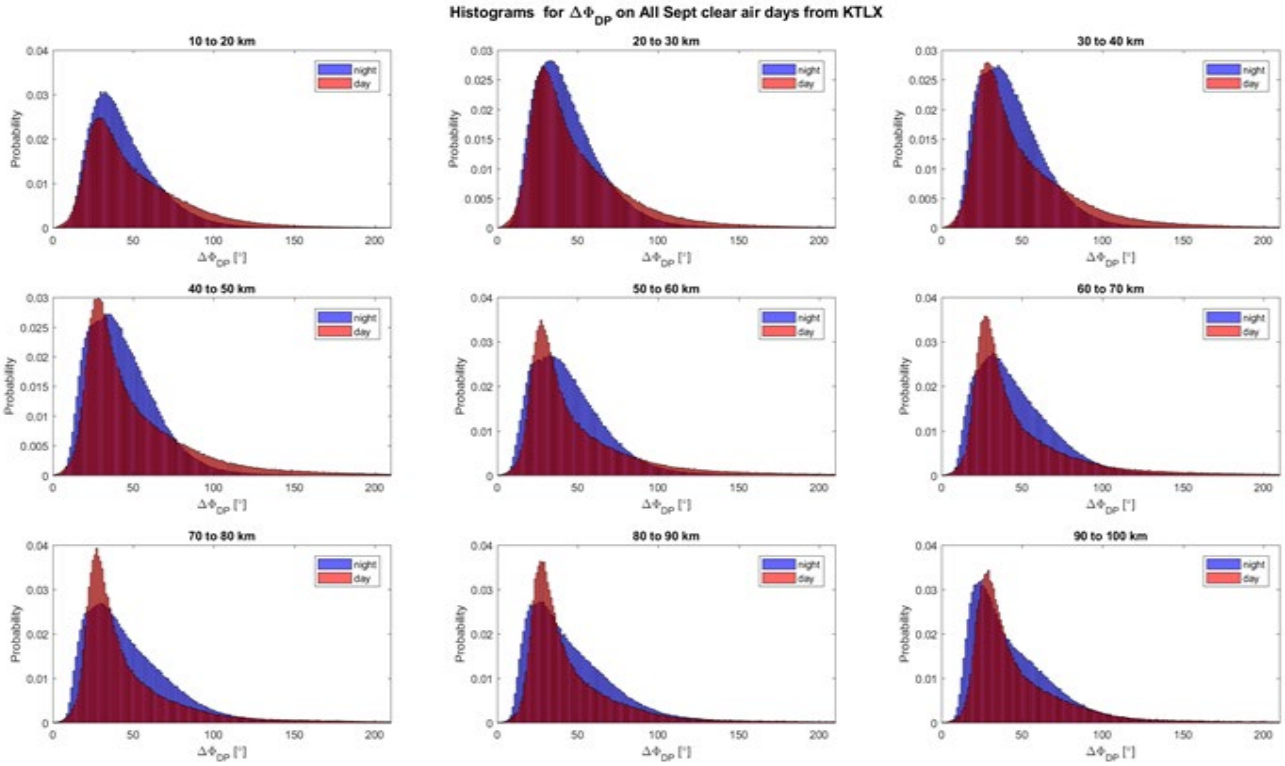

Fig. 3.16. Texture $\Delta\varphi_{DP}$.

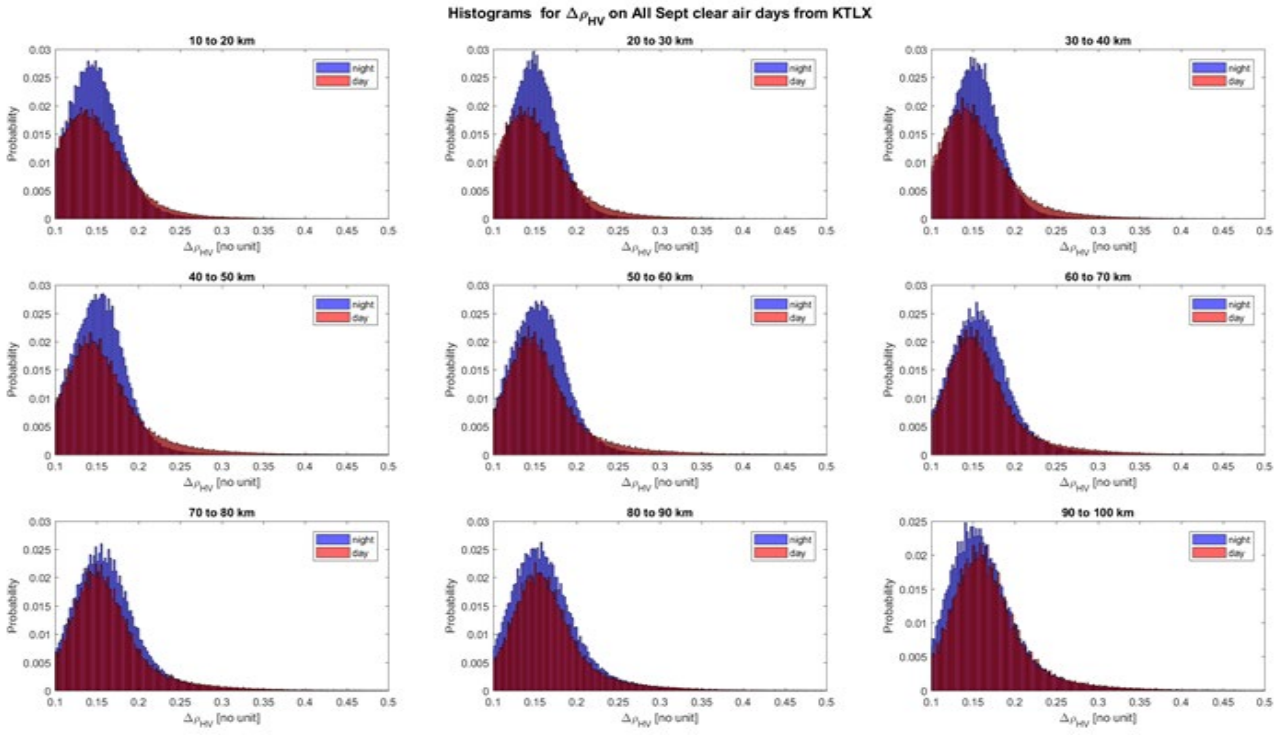

Fig. 3.17. Texture $\Delta\rho_{HV}$.

4. Fuzzy logic algorithm to distinguish bird and insect radar echoes

Most radar classification algorithms work on the principle of fuzzy logic. Decisions are made by comparing measured properties of scatterers with previously acquired knowledge. Final class assignment is based on the level of consistency between the two. Fuzzy logic classification principles for weather radar targets were first explored by Straka and Zrnic (1993) and Straka J. M. (1996). Over time more refined routines have been developed by Zrnic and Ryzhkov (1999), Vivekanandan, et al. (1999), Liu and Chandrasekar (2000), Zrnic et al. (2001), Schuur et al (2003), Keenan (2003), Lim et al. (2005), Marzano et al. (2008), Gourlery et al. (2006) and Krause (2016). A major advantage of fuzzy logic is that it considers many variables so the noise impact is minimized.

The Hydrometeor Classification Algorithm (HCA) by Park et al (2008), currently used on the WSR-88D, applies fuzzy logic to identify various classes of echoes. One of these classes is the "Biological Class", however the algorithm cannot classify its taxa. In this section, we describe a bird/insect fuzzy logic classification scheme based on observation of clear air echoes. Results from the previous section were obtained for the dominant presence of birds during the night and insects in the day. The membership functions are derived directly from the observations. These functions are unique for every 10 km range interval considered.

4.1. General structure of the algorithm

Fig 4.1 below shows the general structure of the algorithm. It uses 7 parameters comprised of five radar products and two texture products; they are Z, σ_v, ZDR, φ_{Dp}, ρ_{HV}, ΔV and $\Delta\sigma_v$. These parameters were chosen based on the quality of separation between bird and insect echoes.

Four classes of clear air echoes are defined. They are birds, insects, unclassified and unknown. The "unclassified" class is assigned for range gates outside the considered range (10 – 100 km) or without adequate radar measurements to make classification. The "unknown" class is assigned just in case gates show equal tendency for both birds and insects i.e when aggregation values for both classes are equal.

The likelihood of a range gate belonging to a class is measured as the aggregation value. An additive aggregation Q_i is computed as (Park et al. 2008, Gourlery et al. 2006)

$$Q_i = \frac{\sum_{j=1}^{7} W_{ij} P^{(i)}(v_j)}{\sum_{j=1}^{7} W_{ij}} \quad , \tag{4.1}$$

where Q_i is the aggregation value of the *i*th class, $P^{(i)}(v_j)$ is the membership of the *j*-th variable to the *i*-th class, and W_{ij} are the weights of the *j*-th variable and *i*-th class.

Additive aggregation is chosen for this algorithm because it is more resistant to noise or abnormal measurements. Other studies (e.g., Liu and Chandrasekar 2000, Lim et al. 2005) use a multiplicative aggregation procedure, however it can be easily biased by values near zero or that are extremely high. Another procedure is the "hybrid" aggregation, used by Zrnic

et al. (2001) and Schuur et al. (2003). However, they have been found to be sensitive to Z biases caused by calibration uncertainties or attenuation (Gourlery et al. 2006).

After the aggregation for each class is computed, the final class is selected as the one with the maximum value. Gates are marked as unclassified if they are outside the considered range (10-100 km), or when the sum of the weights of available (non NaN) variables fails to exceed a threshold of 0.6. This threshold ensures that classification of a range gate proceeds only when the variables available can account for 60% of the total possible weight. Unknown class is assigned for the rare case that aggregation values for birds and insects are equal.

The last step is despeckling. It is unlikely that a radar volume filled with insects will be completely surrounded by birds. Despeckling considers a 3 by 3 window (or texture volume) over the classification output and changes the reference gate to be bird, only if all surrounding gates from the same elevation are classified as birds. So, it is assumed that the reference gate has its non-bird characteristics due to fluctuation of radar returns.

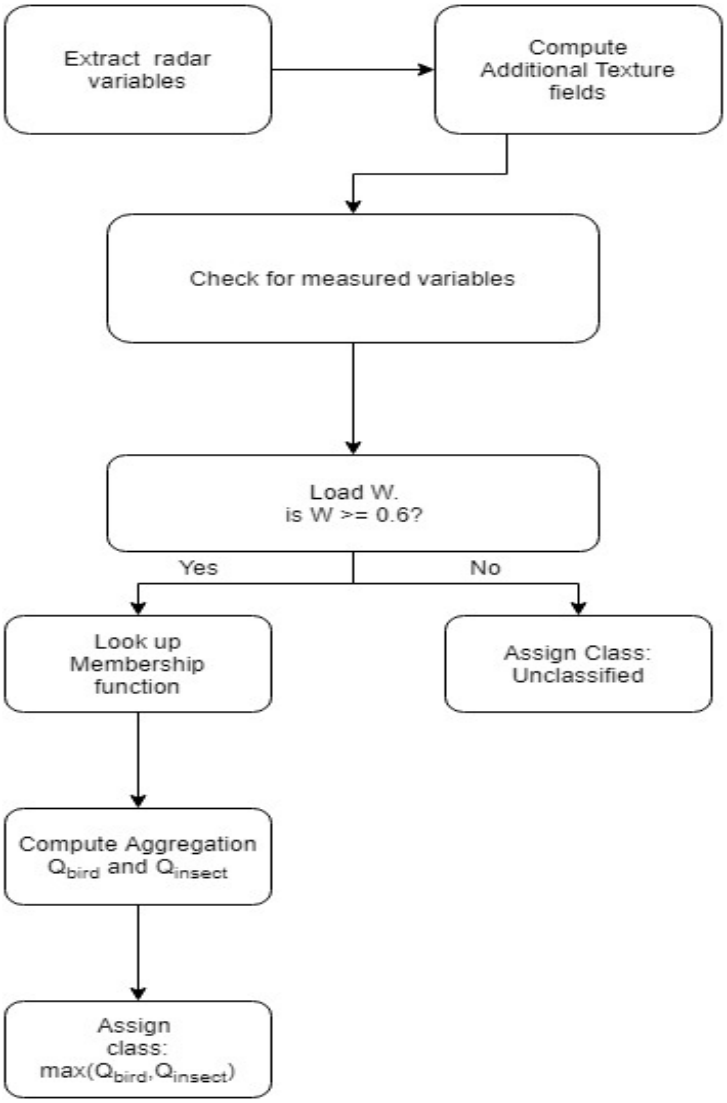

Fig. 4.1. Flow chart of fuzzy logic algorithm.

4.2. Membership functions and weights

The quality of a successful fuzzy logic algorithm depends on how well the membership functions describe the scatterers. Many studies use empirical knowledge or previous observations to form these functions. Zrnic et al. (2001) used trapezoidal shapes to describe observed range of scatterer's values while Liu and Chandrasekar (2000) use continuously differentiable beta functions. In this study, the membership functions are derived directly from the observed distributions for birds and insects. They are computed using the Gaussian kernel density estimation (Silverman 1986, Gourlery et al. 2006) in the following form

$$P^{(i)}(x) = \frac{1}{\sigma\sqrt{2\pi}} \sum_{k=1}^{n} e^{-\left[\frac{1}{2}\left(\frac{x_k - x}{\sigma}\right)^2\right]} \quad , \qquad (4.2)$$

where $P^{(i)}(x)$ is the membership of variable x to the *i*-th class, x_k is the *k*th observation of variable *x*, *n* is the total number of data points, and σ is the bandwidth.

The function $P^{(i)}(x)$ is normalized so that the maximum membership is one before use in the algorithm. The bandwidth σ controls the smoothness of the estimated function. High σ values can lead to a noisy function while low σ values can lead to an over smooth one. The optimal bandwidth is selected using Silverman's rule, i.e

$$\sigma = 1.06\, SD\, n^{-\frac{1}{5}} \quad , \qquad (4.3)$$

where SD is the standard deviation of the observed variable *x*. The resulting function is essentially a smoothed histogram of the radar data. Fig 4.2 – 4.8 show the membership functions for ΔV, $\Delta\sigma_v$, φ_{Dp}, ρ_{HV}, σ_v, ZDR, and Z respectively. Densities for birds are in blue while those for insects are red.

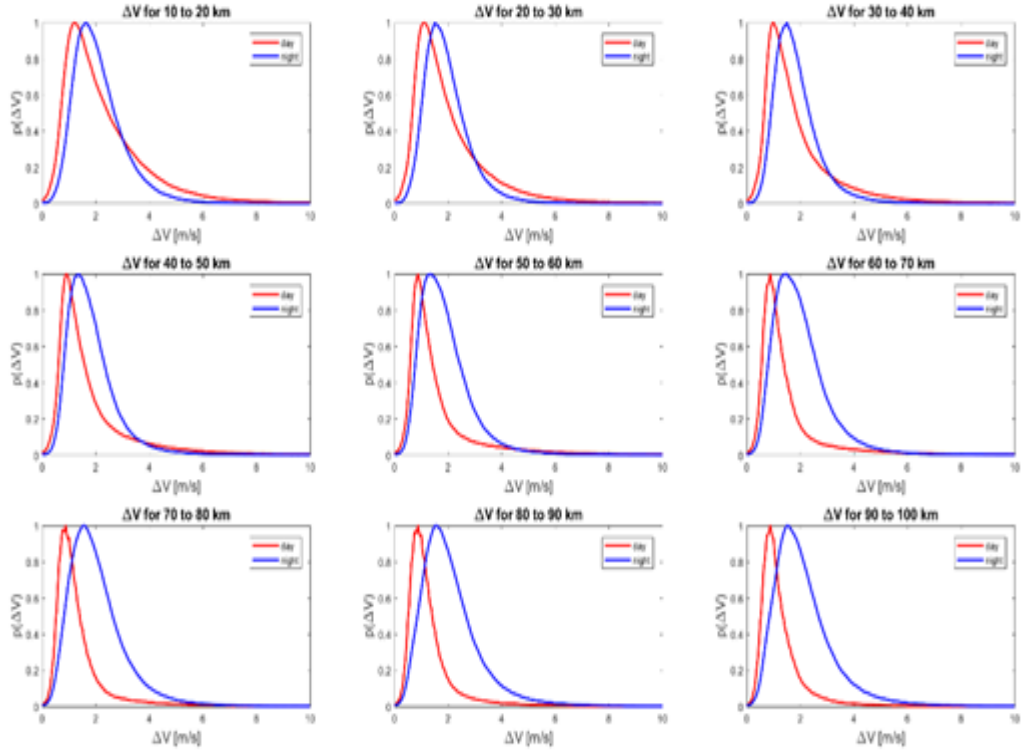

Fig. 4.2. Membership functions for ΔV.

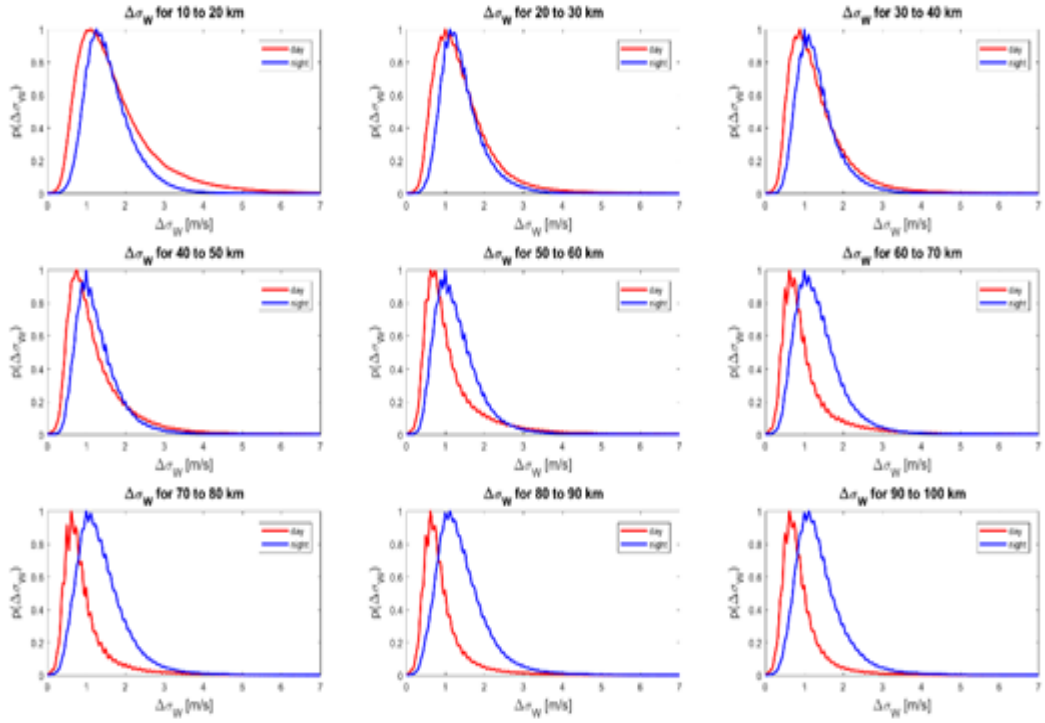

Fig. 4.3. Membership functions for $\Delta\sigma_v$.

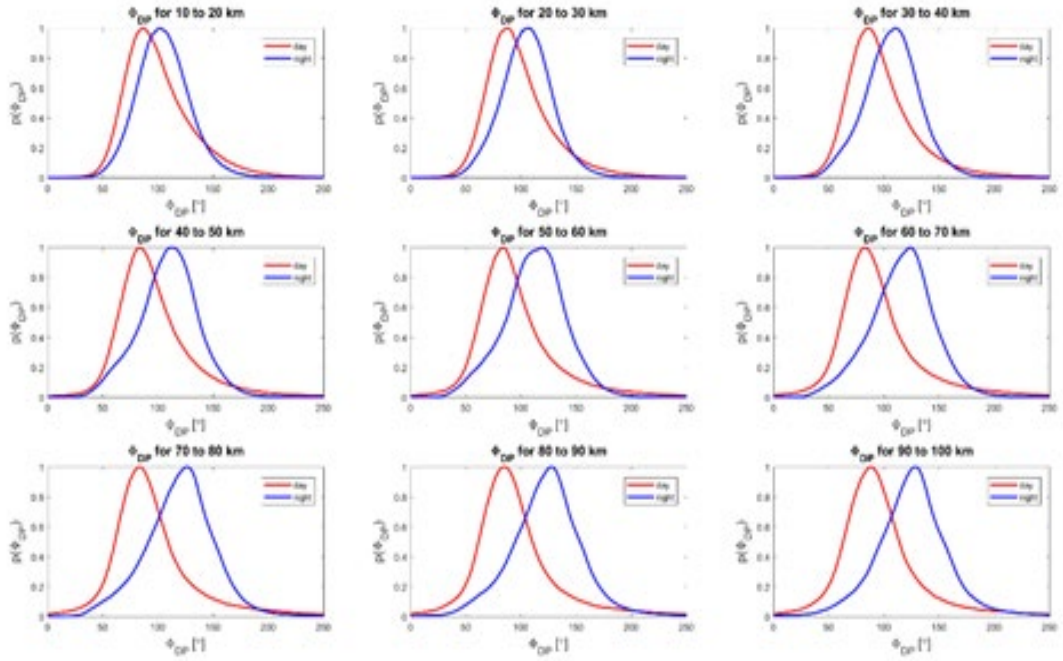

Fig. 4.4. Membership functions for φ_{DP}.

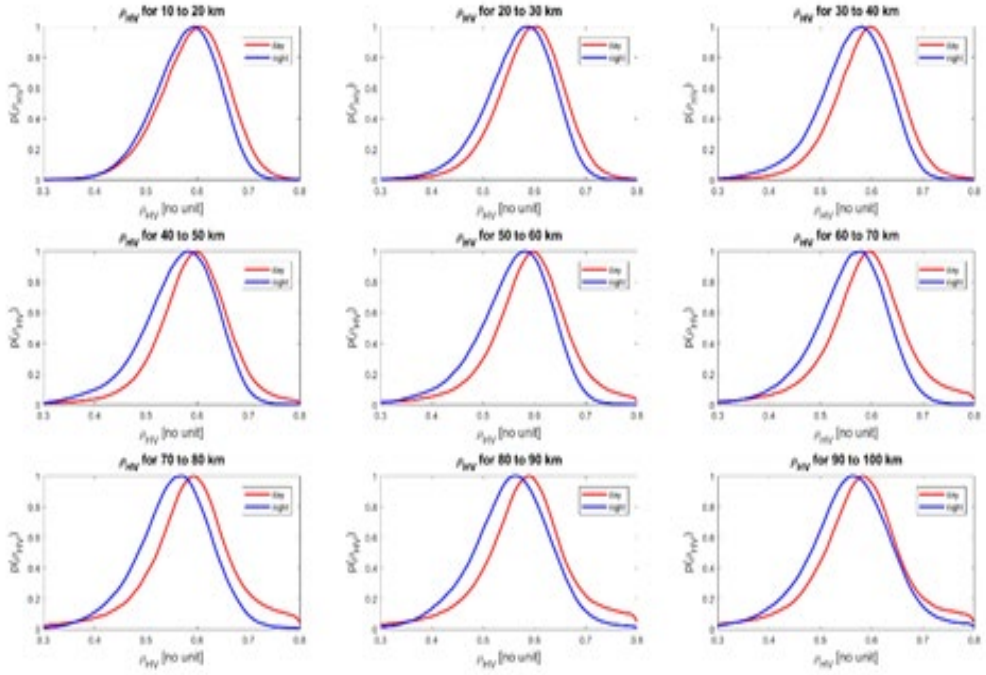

Fig. 4.5. Membership functions for ρ_{HV}.

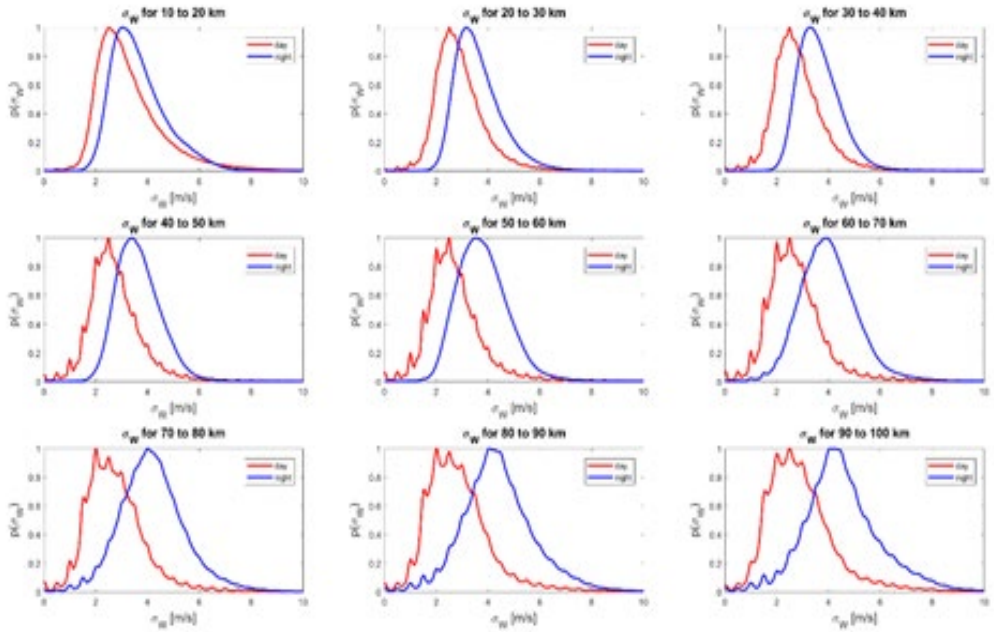

Fig. 4.6. Membership functions for σ_v.

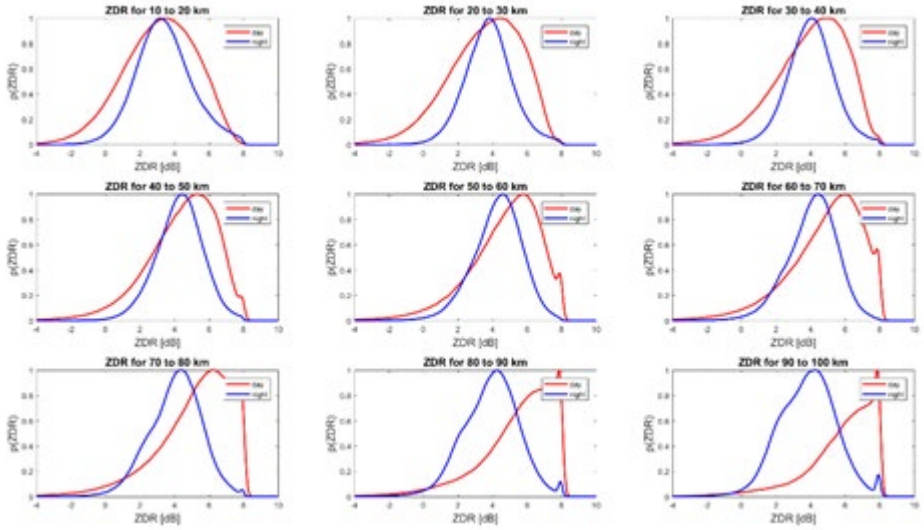

Fig. 4.7. Membership functions for *ZDR*.

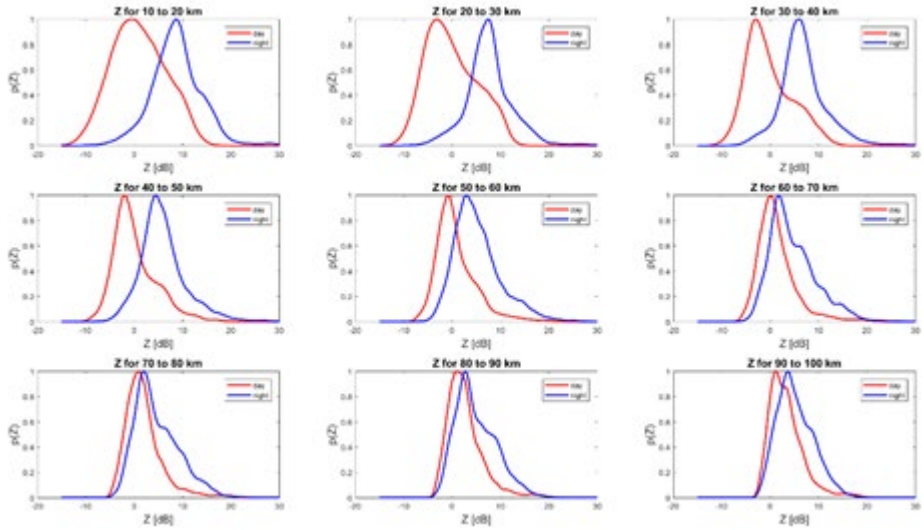

Fig. 4.8. Membership functions for *Z*.

The weights defined in (4.1) determine the extent each variable play in the classification procedure. They were computed based on the degree of overlap between the density of the two classes (Park et al., 2007). If a variable has strong overlap between bird and insect density, it is assigned a low weight and vice versa. For example, Fig. 4.9 shows the distribution for φ_{DP} at the 40 -50 km range. The overlapping region, A (highlighted in pink) was found to be 0.68. This procedure was repeated for all *j* variables at the same range. The final weights are estimated as

$$W_j = \frac{1}{A_j} \sum_{j=1}^{N} \frac{1}{A_j} \quad , \tag{4.4}$$

where N is the number of variables considered. All weights for each range interval are normalized so they sum to one. Table 2 below shows the weights for all variables and ranges considered.

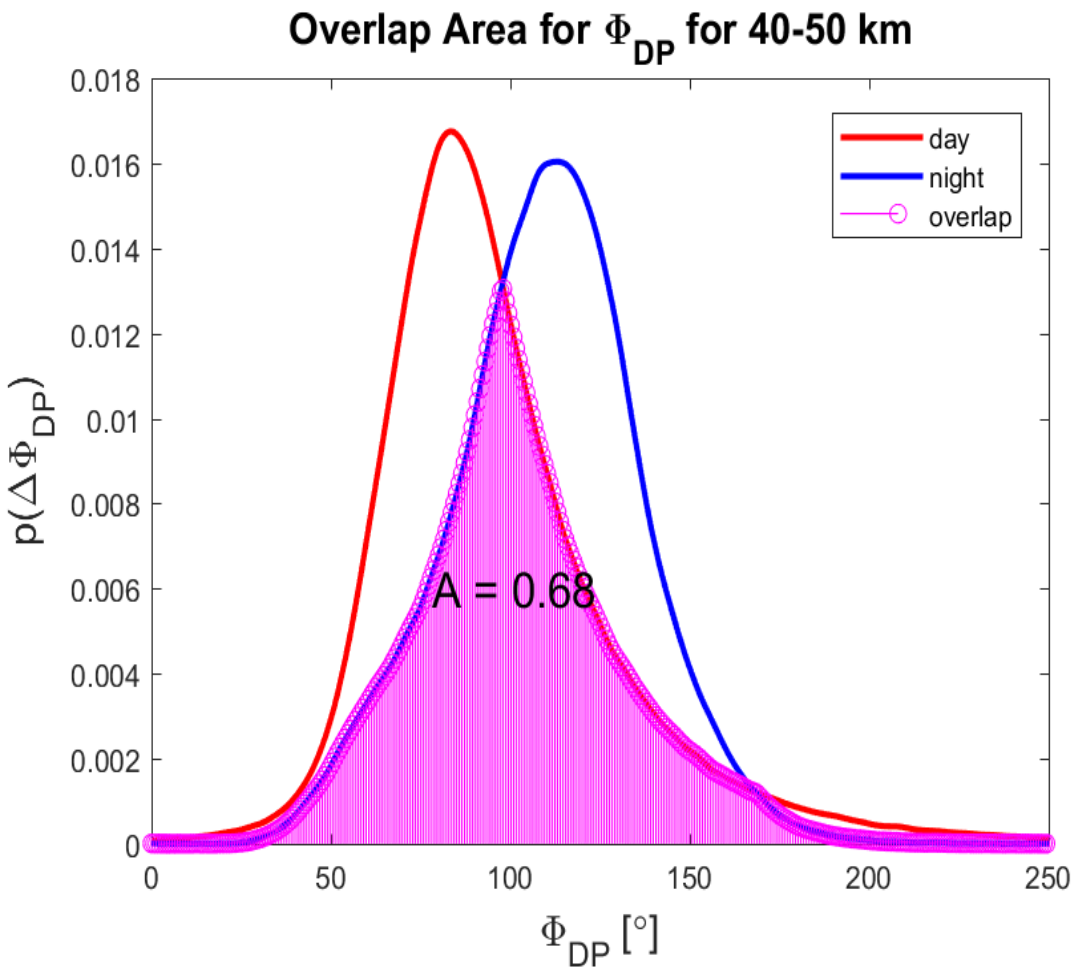

Fig. 4.9. Area of Overlapping region for φ_{DP} for 40 – 50 km.

Table 2. Weights of all variables and ranges.

	Range (km)									
Parameter		**10 – 20**	**20 - 30**	**30 - 40**	**40 - 50**	**50 - 60**	**60 -70**	**70 - 80**	**80 - 90**	**90 - 100**
	ΔV	0.13	0.13	0.13	0.13	0.13	0.13	0.13	0.13	0.13
	$\Delta\sigma_v$	0.1302	0.1152	0.1127	0.1185	0.1289	0.14	0.1486	0.1515	0.1483
	φ_{DP}	0.1306	0.1283	0.1309	0.1396	0.1491	0.1542	0.1558	0.1564	0.1541
	ρ_{HV}	0.1163	0.1115	0.1121	0.1111	0.1116	0.1096	0.1074	0.1002	0.0932
	σ_v	0.1363	0.153	0.1638	0.1713	0.1798	0.183	0.1787	0.1766	0.1731
	ZDR	0.1257	0.1283	0.1248	0.1217	0.1254	0.1336	0.1399	0.1535	0.1724
	Z	0.2309	0.2384	0.2329	0.211	0.1686	0.1344	0.1205	0.1116	0.1082

5. Classification results

5.1. Insect test cases

Dates for the insect test cases were obtained from the US Department of Agriculture (USDA) in Texas which monitors the activity of insects in many states including Oklahoma. A large population of Monarch butterfly, *Danaus plexippus* was confirmed on 19th July, 2013, 17 -19 UTC (12 – 14 CDT) and 1st November, 2013, 22 -23 UTC (17-18 UTC). Also, the input variables were obtained by combining variables from cut 1 and Z, V and σ_V from cut 2. This approach is effective for studying a wide coverage of homogenous taxa (radar volume is mostly birds or mostly insects). A modification to enable the classification of finer and more localized features of bird/insect migration is presented in the next section.

For the July 2013 case, the algorithm was applied to a PPI from KLTX collected 12:46:04 CDT. The classification result is shown in Fig 5.1. The algorithm detected 87.9 % of echoes to insects and 12.1 % to be birds. This correlates with the USDA's observation of a large population of Monarch butterflies. It can also be observed that birds are mostly isolated echoes consistent with the tendency for birds to aggregate within one resolution volume. Results for 17:30:06 CDT on 1st November, 2013 is shown in Fig. 5.2. Insects were also found to dominate echoes at 76.5%. Bird echoes are also seen as isolated targets.

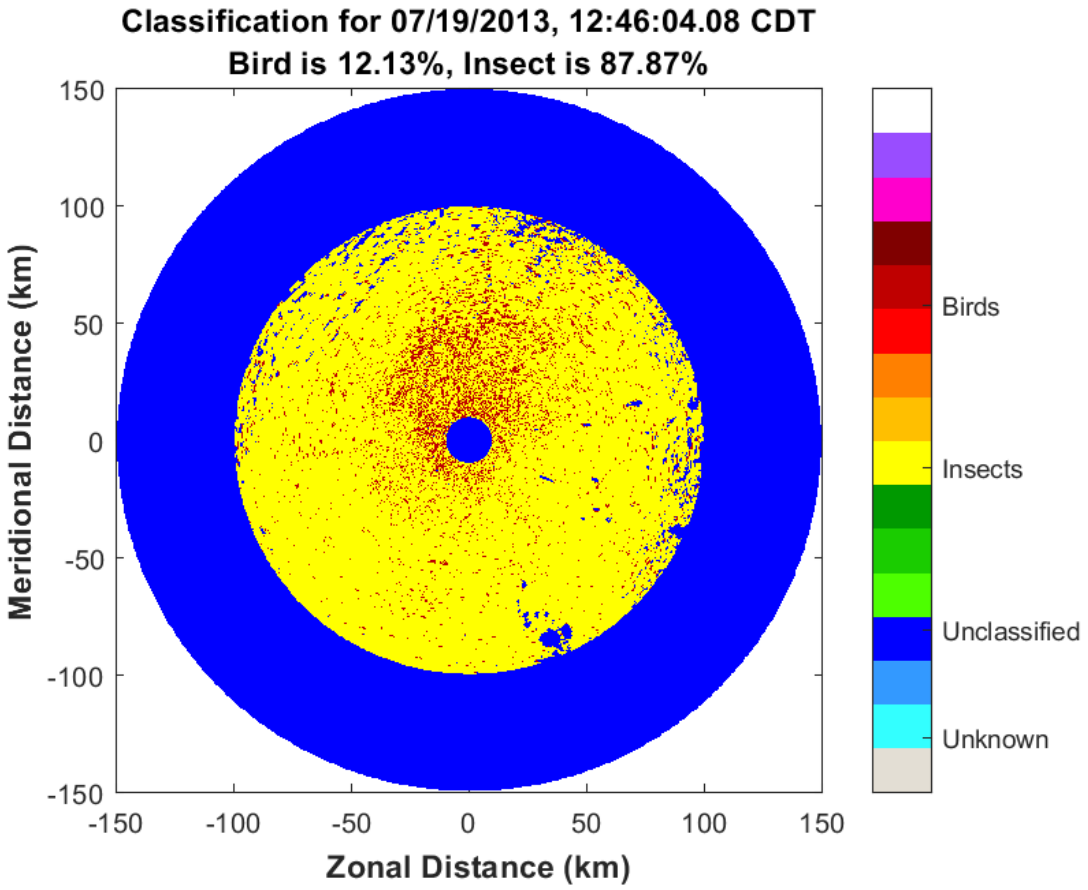

Fig. 5.1. Classification result for 19th July, 2013 at 12:46:04 CDT.

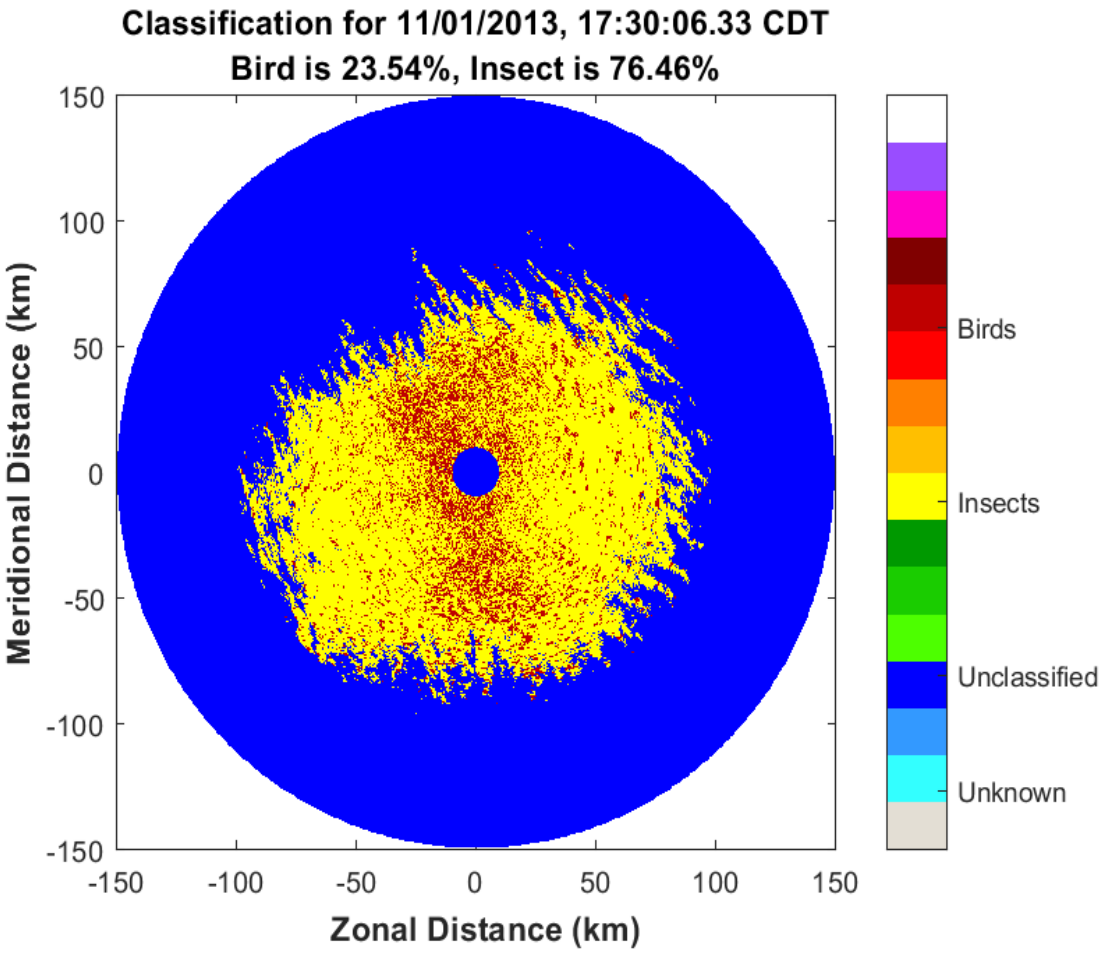

Fig. 5.2. Classification result for 1st November, 2013 at 17:30:06 CDT.

5.3. Bird test cases

Testing of the bird/insect detection algorithm for dominant species was carried out on data from 0 UTC to 23 UTC on 17^{th} September, 2015 (see section 5.4). Results obtained were consistent with birds dominating night time echoes and insects dominating day time echoes. While this method is effective for studying a wide coverage of homogenous taxa (radar volume is mostly birds or mostly insects), classifying finer and more localized features of bird/insect migration will be a challenge.

In this section, a classification approach using only variables from cut 1 and reasonable thresholds is explored. The variables used are Z (cut 1), ZDR, ϕ_{DP} and ρ_{HV}. Before final class assignment, a threshold of $ZDR = 7.6$ dB is imposed. This was selected because insects have been observed to have ZDR values accumulating on the 8.0 dB maximum that the WSR - 88D radar can measure compared to much lower values for birds. Thus values exceeding this threshold are very likely insects. A final threshold of $\rho_{HV} = 0.95$ is applied to exclude possible contamination by weather

The modified algorithm was tested on two well-known bird cases. The first case shown in Fig .5.3 was collected from KTLX between 11 to 12 UTC on 8^{th} August, 2017. The panels from left to right, top to bottom show emanating rings of reflectivity seen as birds leave their roosting sites. The rings are enclosed in the yellow circles. The rings north – west of the KTLX radar has been confirmed to be purple martins. The modified bird/insect classification algorithm was applied to these cases. The results are shown in Fig. 5.4. Range gates with birds are colored red, insects – yellow, weather - green and unclassified gate – blue. The algorithm accurately detects birds as the cause of these reflectivity rings. They are shown enclosed in the black circles. It should also be noted that corresponding panels in Fig 5.3 and 5.4 are the same PPI. There is thus an obvious correlation between the known location of the rings (enclosed in yellow) and the rings detected by the algorithm (enclosed in black).

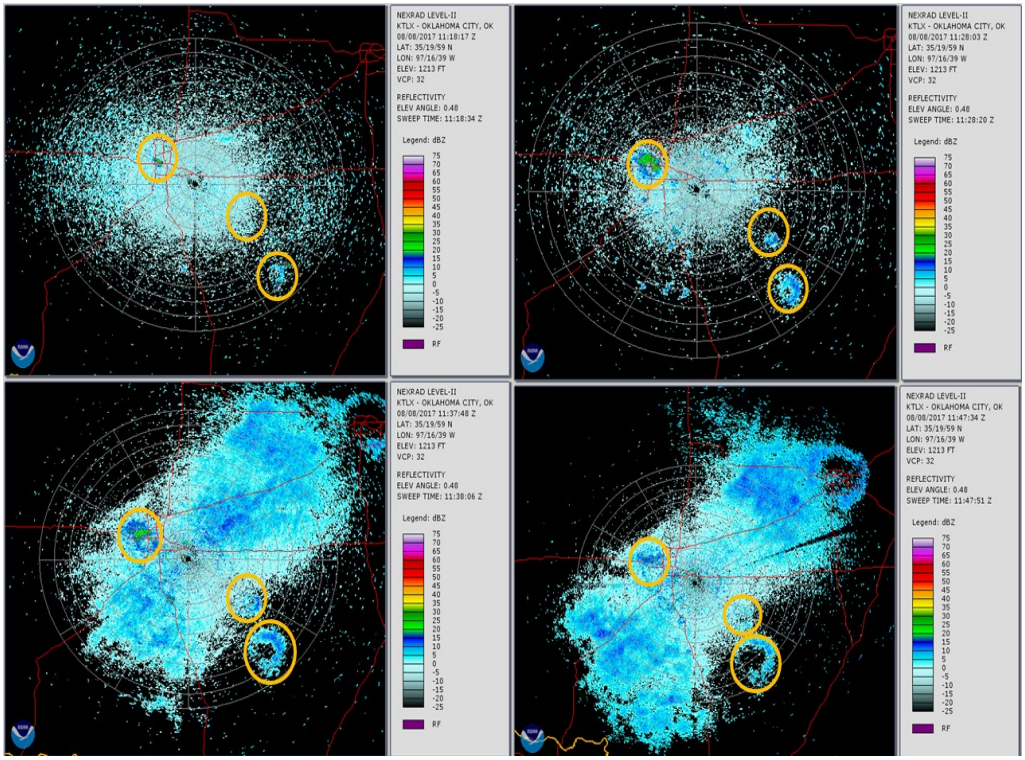

Fig. 5.3. PPI's for 11 to 12 UTC on 8th August 2017. The parts enclosed in the yellow circle are observed bird.

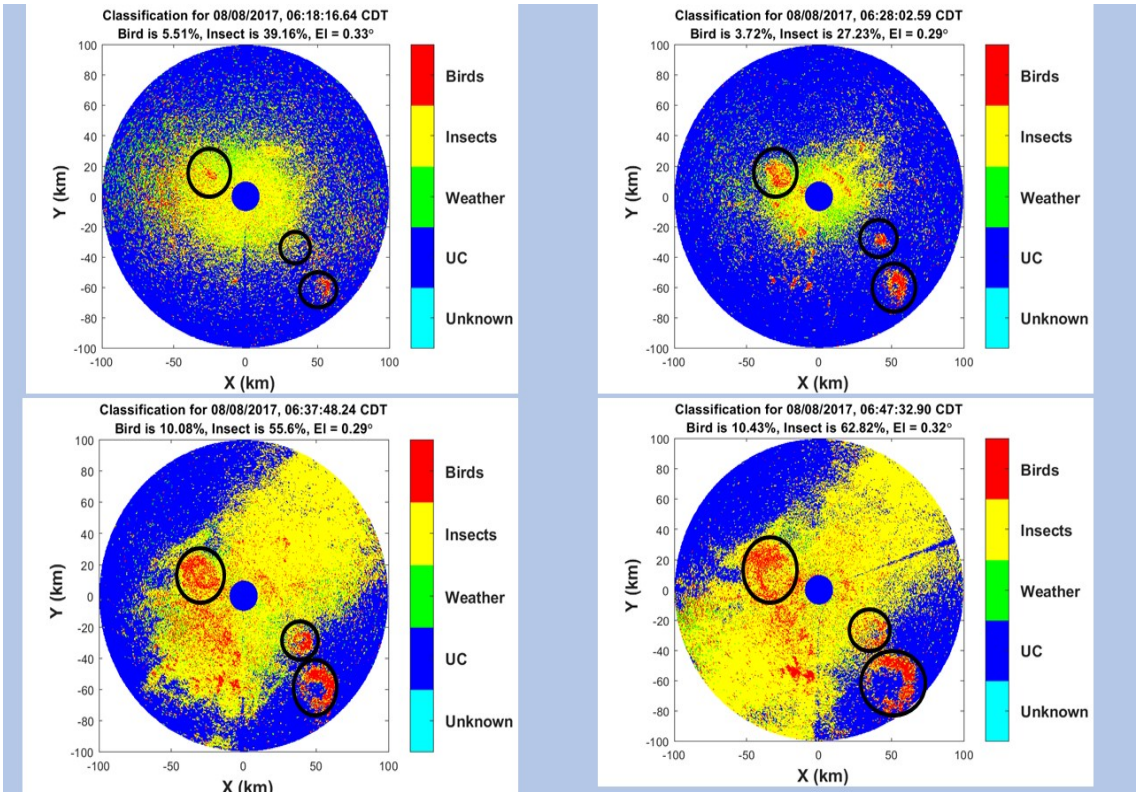

Fig. 5.4: Classification results for Fig. 5.3. Birds are in red while insects are in yellow. Algorithm correctly identifies bird rings.

The second test case was also collected from KTLX from 4 to 11 UTC on 3rd March, 2018. On this day the temperature was too cold for insects to fly out so most clear air echoes observed were birds. Reflectivity from 23 CDT on 2nd March, 2018 to 4 UTC on 3rd March, 2018 are shown in Fig. 5.5. Fig. 5.6 shows the classification results for the corresponding panel in Fig. 5.5. Most gates are classified as being bird dominated consistent with the observation that birds are the major cause of these echoes. The first panel collected at 23:51:00 CDT on 2nd March 2018 has 82.2% of echoes classified as birds. The percentage of birds detected reduces to 53.7% as morning approaches that is consistent with dawn insect take off. It can also be seen that many insects are detected in the gates at the lowest height (enclosed in the black circle in Fig. 5.6). This is consistent with the known behavior of birds to fly at higher altitudes compared to insects.

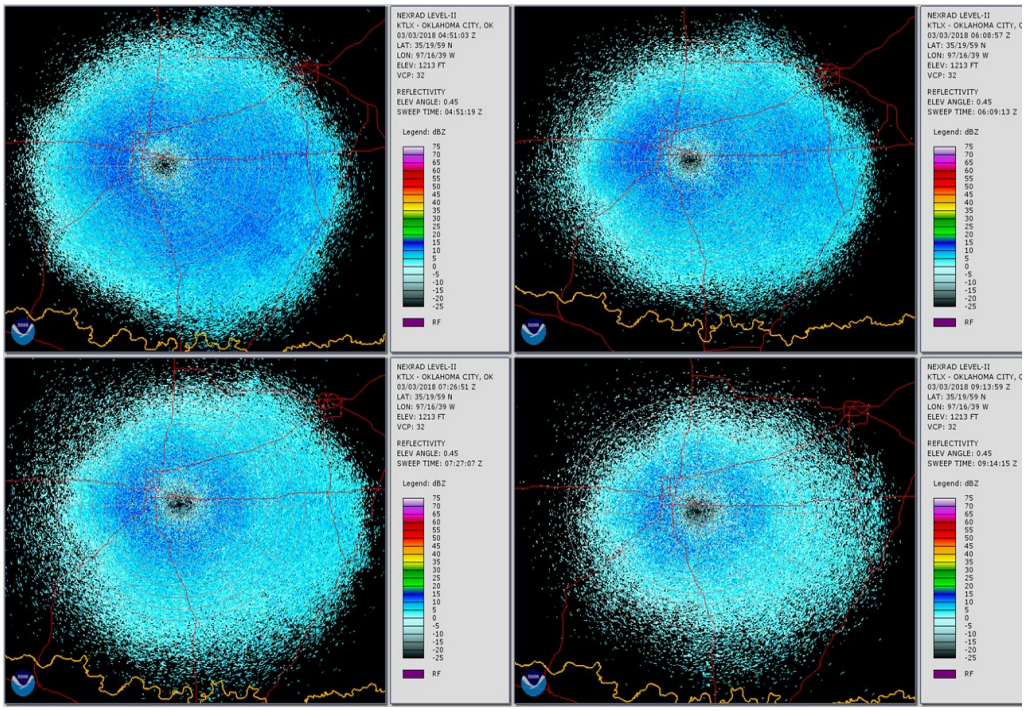

Fig. 5.5. Reflectivity for 23 CDT on 2nd March, 2018 to 4 UTC on 3rd March, 2018.

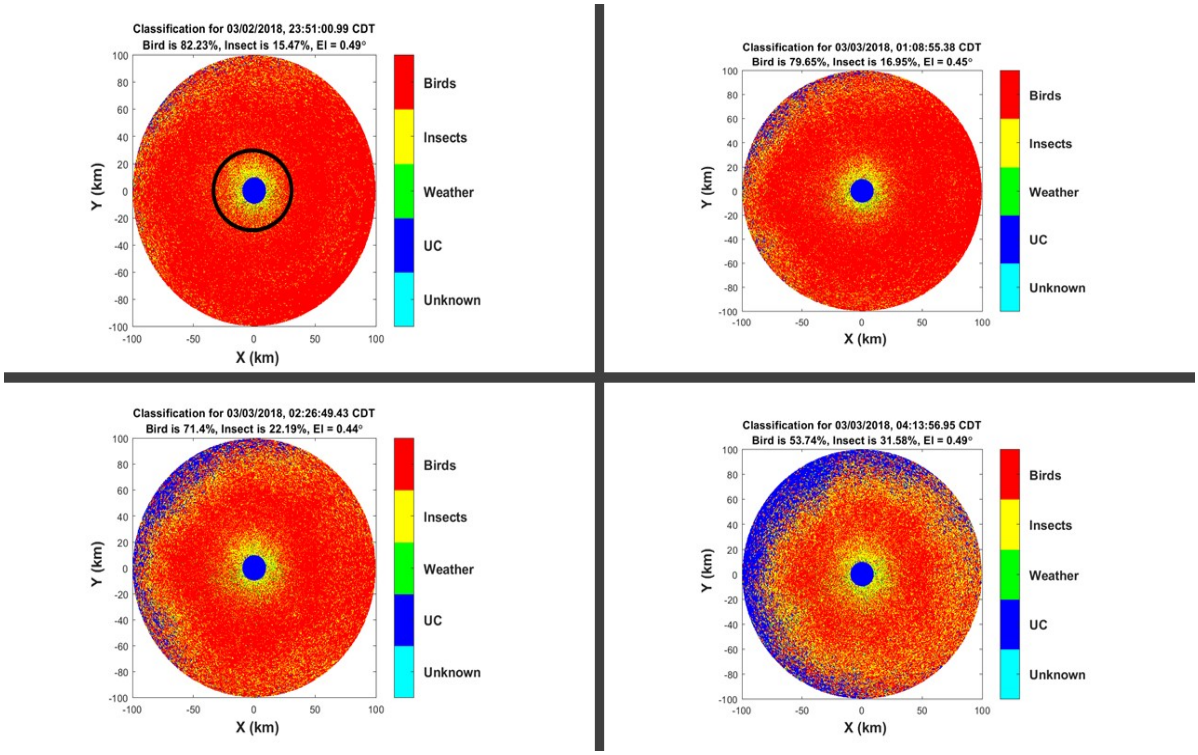

Fig. 5.6. Classification results for PPI's in Fig. 3 above. Most gates are classified as birds (red). Gates close to the radar are classified as insects shown in the black circle.

5.2. Daily cycle case

Observations of clear air Reflectivity show a daily cycle (Martin, 2003) with dips at sunrise and sunset and clear change in scattering mechanism between day and night. In this section data from a 24-hour cycle, between 19 CDT on 16th September, 2015 and 18 CDT, 17th September, 2015 is classified to explore this cycle. The results are presented in Fig 5.7 – 5.10.

Insects initially dominate echoes with 81.9% at 19 CDT for the first day (Fig. 5.7) but soon after its area decreases till it dips at 3 CDT, the next day with 51.1%. (Fig. 5.8). After this point, insect percentage rises continuously till it reaches its maximum at 9 CDT (early morning) with 93.2%. Generally, day time (9 CDT to 18 CDT), insect percentage is high with 85.7% seen in Fig. 5.9 and 5.10. Night time (21 CDT to 6 CDT) on the other hand, has lower insect percentage of 59% seen in Fig 5.7 and 5.8. Day break (6 CDT) is observed to be the inflection point with 71% of echoes identified as insects

Bird abundance rises from 18% at 21 CDT on 16th September 2017 (Fig. 5.7). This trend continues up till 4 CDT (Fig. 5.7) the next day with 46.8%. Peak values are recorded at night (between 21 CDT and 4 CDT) with an average of 43.3% seen in Fig. 5.7 and 5.8. After this point, bird percentage falls for the rest of day time. 9 – 18 CDT have generally low values with an average of 14.3%. These results show that insects dominate day echoes while birds dominate nocturnal echoes. Results also show a distinct change in behavior of birds and insects at sunrise (6 CDT) and sunset (18 CDT).

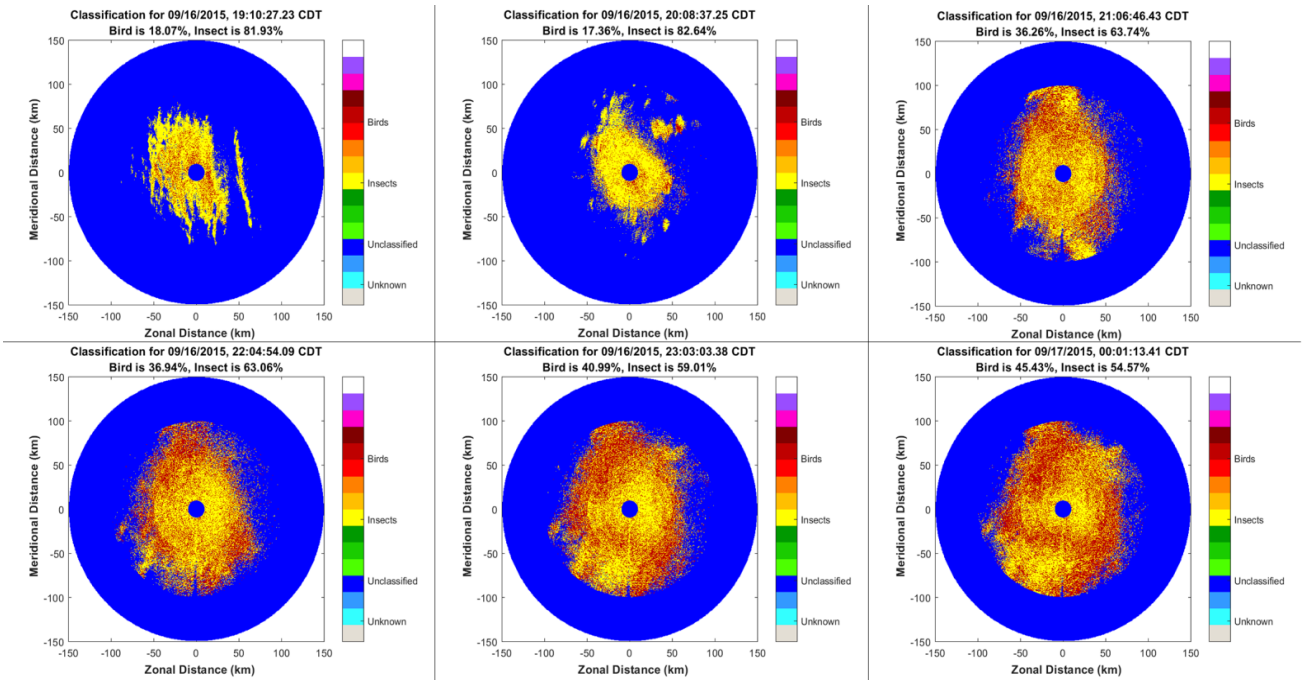

Fig.5.7. Classification result for19 CDT, 16 September, 2015 to 1 CDT, 17 September, 2015.

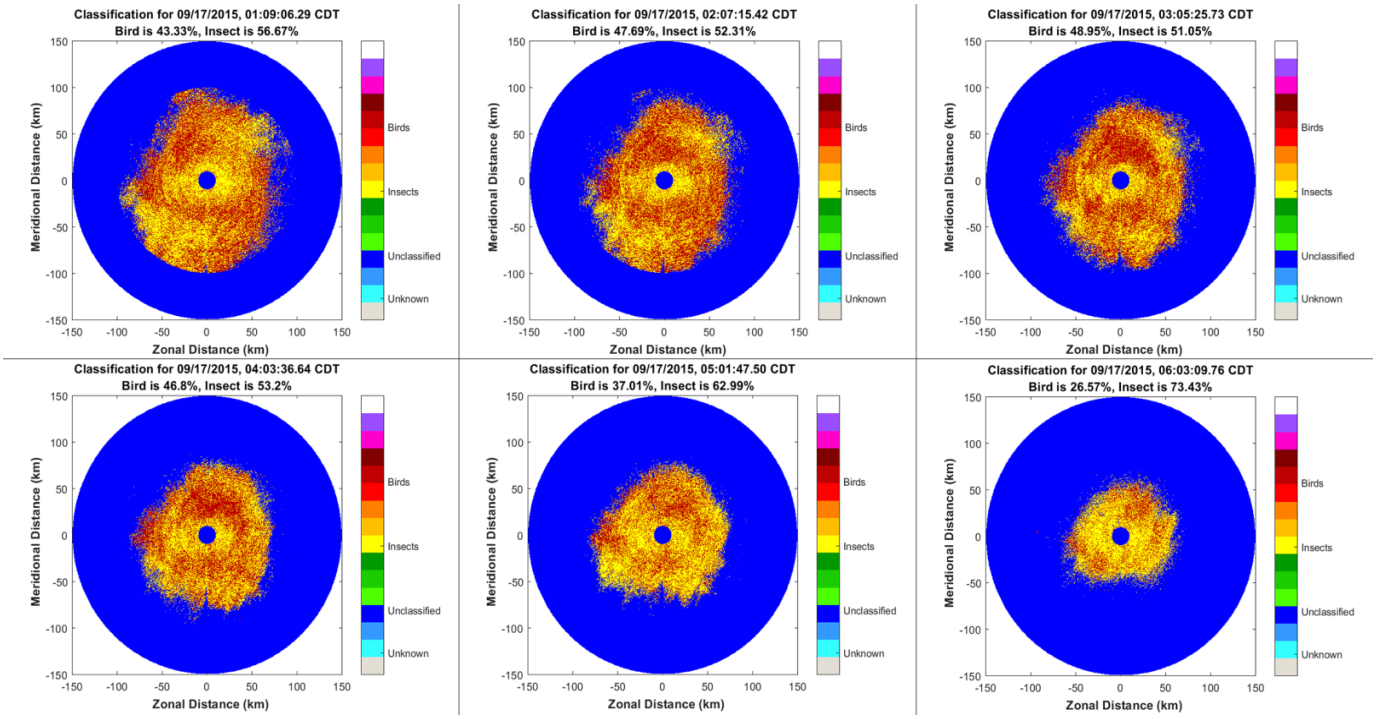

Fig. 5.8. Classification result for 17 Sept, 2015, 1 CDT to 6 CDT.

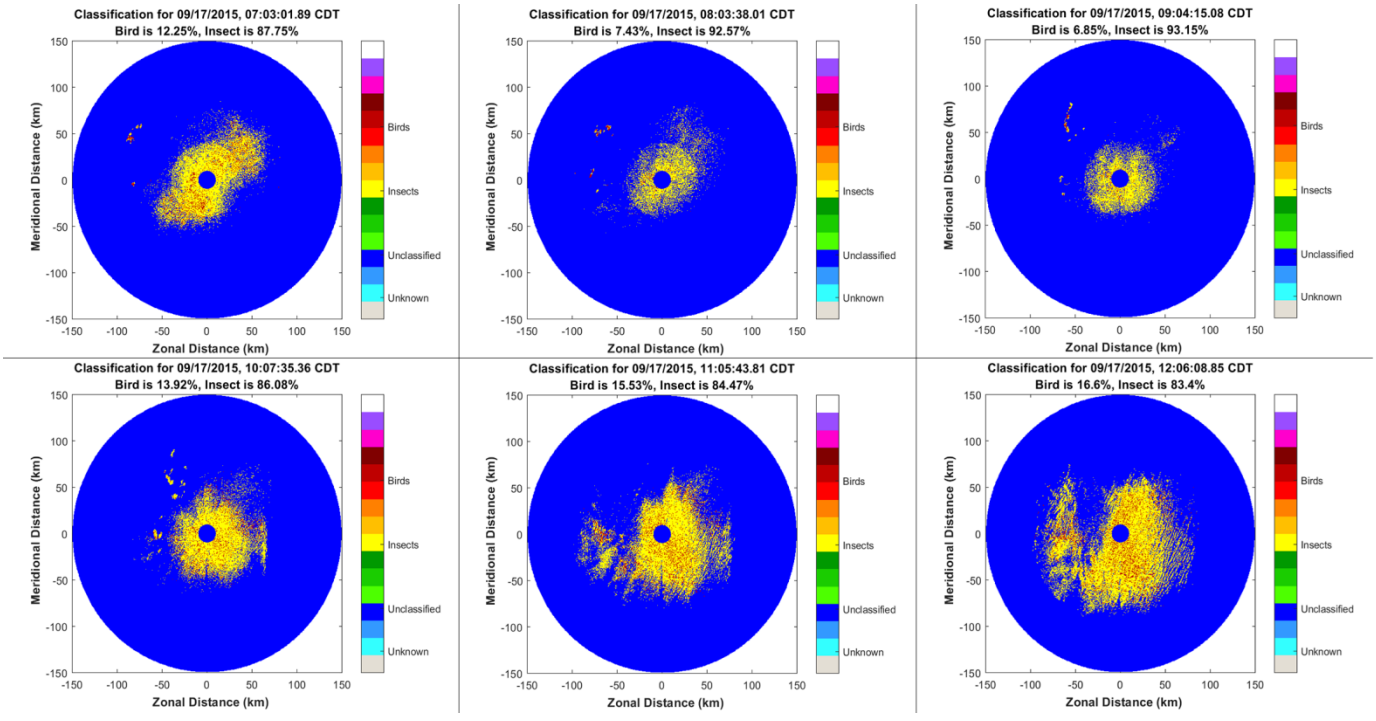

Fig. 5.9. Same as Fig. 5.8, but for 7 CDT to 12 CDT.

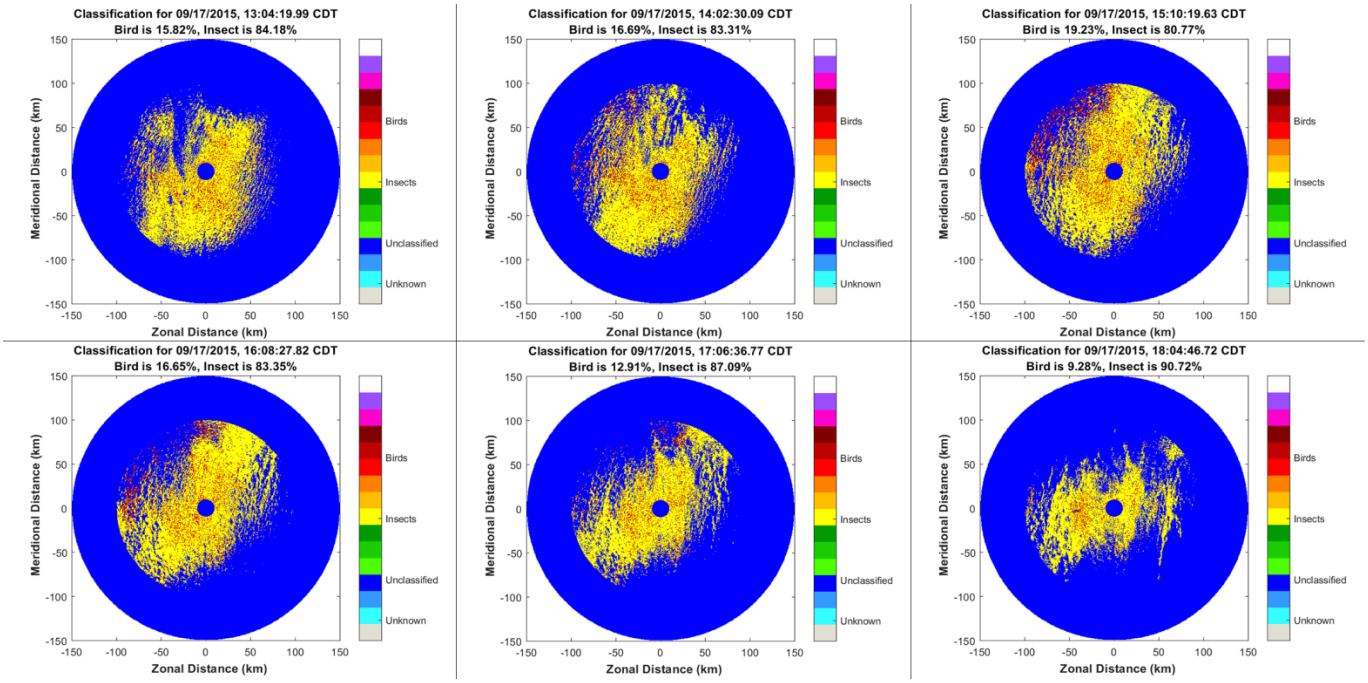

Fig. 5.10. Same as Fig. 5.9, but for 13 CDT to 18 CDT.

6. Summary and conclusions

Current WSR-88D's Hydrometeor Classification Algorithm (HCA) does not distinguish radar echoes from birds and insects. The HCA currently has one class "Biological" for flying birds, bats, and insects. The recognition of bird and insect radar echoes is important for meteorology, aviation, ecology, biology, and agriculture. The WSR-88D radars estimate the wind velocities using observations in "clear air", i.e., in situations free from precipitation. The Velocity-Azimuth-Display (VAD) technique is used for that. Birds are active flyers and their velocities deviate from the wind significantly. Therefore the Doppler velocities of birds cannot be used for the estimation of the wind. On the other hand, insects are almost passive flyers and they may be used as wind tracers. Selecting radar resolution volumes with insects can be useful for meteorology for the wind estimation via the VAD. Flying birds are a major hazard for aviation while insects are benign. Therefore the radar detection of birds can be useful in preventing collisions of birds with aircrafts and helicopters.

The dual polarization WSR-88Ds deliver 6 radar variables for each radar resolution volume: reflectivity (Z), Doppler velocity (V), spectrum width (σ_v), differential reflectivity (ZDR), differential phase (φ_{DP}), and correlation coefficient (ρ_{HV}). Our radar observations in "clear air" show that the values of radar variables change with range from radar. This is probably because various species fly at various heights. Therefore the range dependence should be included into an algorithm for distinguishing bird and insect echoes. We have limited our analysis by ranges up to 100 km where the range dependence of radar variables is sufficiently strong. The developed algorithm could be applied for an airport terminal area, which is 50-60 km from an airport, if the WSR-88D is sufficiently close to the airport.

It is known from ornithology and entomology that in the migration periods, birds fly primarily at night and insects may fly throughout the day, but preferable flight time is during the day. Data collected from clear air days have been analyzed at daytime and nighttime. The distributions of the values of all 6 radar variables and their spatial textures have been obtained for 22 days in September 2017 for day and night times. Birds are larger, faster, fly more independently, and have greater variation in the mentioned features compared to insects. These properties are observed with the distribution of nocturnal echoes having a higher median Z, V, σ_v, φ_{DP} and lower median ρ_{HV} than the day echoes. The spatial texture ΔV and $\Delta\sigma_v$ which measure the spatial variability of scatterer velocities are also higher for night time providing more evidence in favor of bird abundance in nocturnal echoes.

The distributions of all 6 radar variables and corresponding 6 spatial textures ΔZ, ΔV, $\Delta\sigma_v$, $\Delta\varphi_{DP}$, ΔZDR, and $\Delta\rho_{\mathrm{hv}}$ have been obtained for the nights and days. After data analysis, a fuzzy logic classification algorithm is developed to delineate birds and insects in clear air echoes. The membership functions are derived using the Gaussian kernel approximation on observed data. Weights are objectively defined using the degree of separation between classes, so that parameters that show the clearest separation between night and day have the most effect on classification. Five radar products (Z, ZDR, σ_v, φ_{DP} and ρ_{HV}) as well as two derived products ΔV and $\Delta\sigma_v$ were chosen for use in the algorithm based on observed separation between distributions of classes.

The following new features have been utilized in the algorithm:

- Range dependence for the radar variables and their textures has been considered,
- All 6 available radar variables and their spatial textures have been analyzed,
- Five radar variables and two texture parameters have been found to contribute the most to the separation of radar echoes from birds and insects,
- Probabilities (distributions) of certain radar variables have been obtained for 6 parameters and their 6 textures,

The algorithm was tested on emanating rings of reflectivity caused by early morning bird take off between 11 to 12 UTC on 8^{th} August, 2017. These rings were correctly identified as bird echoes. Further tests were also carried out on data from 4 to 11 UTC on 3rd March, 2018. On this night, the temperature was too cold for insects to fly, so clear air echoes must be birds. Up to 82.2 % of echoes were classified as birds. This percentage continually dropped as sunrise approached, and an increasing number of insects started taking off.

Further tests were performed on two confirmed cases with a high population of Monarch butterfly, *Danaus plexippus* on 19th July, 2013, 12:46:04 CDT and 1st November, 2013 on 17:30:06 CDT. Data was obtained from the US Department of Agriculture (USDA) in Texas which monitors insect activity in many states including Oklahoma. For the July case, 87.9% of echoes were .classified as insects while 12.1% were classified as birds. For the November case, 76.5% of echoes were classified as insects and 23.5% were classified as birds. Insect echoes were also distributed over large volumes while birds occurred mainly as isolated volumes. It is reasonable to expect birds to be in some resolution volumes. It is

impossible to determine an exact probability of detection since the taxa could not be confirmed from other independent sources.

The algorithm was also tested for a 24-hour period between 19 CDT on 16th September, 2015 and 18 CDT, 17th September, 2015. Insects were found to dominate echoes between 9 CDT and sunset on 17th September, 2015 with an average of 85.7% of classified echoes. After sunset on 16th September, insect percentage falls rapidly with lowest values between 21 CDT and 6 CDT, with an average of 59%. Bird abundance peaked between 21 CDT on 16th September, 2015 and 4 CDT the next day with an average of 43.3%. After sunrise, bird abundance falls rapidly throughout the rest of day time (9 -18 CDT) with an average of 14.3%. A major feature of these results is that day break (6 CDT) marks the inflection point between high and low values for birds and insects. These findings explain the daily cycle of reflectivity observed by (Martin, 2003). Insects are clearly most abundant during the day and birds during the night at migration periods. Sunrise and Sunset are also found to be inflection points in the dominance of birds or insects in the atmosphere.

A few areas can be improved upon in future studies. The wind contributes a lot to measured radial velocity and birds/insects have distinct behavior in relation to the wind. A new algorithm parameter can be derived for the deviation of radial velocity from wind velocity. It is expected that birds will have higher values than insects. Furthermore, the radar variables as functions of azimuth can be reoriented relative to the wind before data processing to properly characterize their dependence on the wind. Independent sources of information about birds and insects in the radar resolution volume are also needed. A camera on an unmanned aerial vehicle could be very helpful for the verification of scatterers in the radar resolution volume.

Acknowledgments

We thank Mr. Adam Heck from the Radar Operations Center (ROC) for writing the WSR-88D level II reader used in this project and Ms. Lindsey Richardson (ROC) for modifying this reader. We also thank Mr. Richard Murmnan (ROC), Mr, Daniel Berkowiz (ROC), and Mr. Donald Burgess (NSSL/CIMMS) for valuable discussions on the algorithm and the results.

References

Bachmann, S., and Zrnic, D. 2006: Spectral Density of Polarimetric Variables Separating Biological Scatterers in the VAD Display. *J. Atmos. Ocean. Technol.* 24, 1186 - 1198.

Battan, L.: 1973. *Radar Observations of the Atmosphere.* University of Chicago Press.

Browning, K., and Atlas, D. 1966: Velocity characteristics of some clear-air dot angels. *J. Atmos. Sci*, 592-604.

Bunch W, and E.E. Herricks, 2010: Observational validation of avian radar systems. In: Proceedings 2010 FAA worldwide airport technology transfer conference, Atlantic City. http://www.airporttech.tc.faa.gov/Airport-R-D/Conference-and-Workshop/Airport-RD-Conference-Detail/dt/Detail/ItemID/229/Observational-Validation-of-Avian-Radar-Systems

Chilson, P.B., W. F. Frick, J. F. Kelly, K. W. Howard, R. P. Larkin, R. H. Diehl, J. K. Westbrook, T. A. Kelly, T. H. Kunz, 2012: Partly cloudy with a chance of migration: Weather, radars, and aeroecology. *Bull. Amer. Meteor. Soc.* **93**, 669–686.

Crawford, A. B. 1949: Radar reflections in the lower atmosphere. *Proceedings of the I.R.E.*, pp. 404-405.

Doviak, R., and Zrnic, D., 1993: *Doppler Radar and Weather Observations. Second Edition.* New York: Dover Publications, 562 pp.

Drake, V. A., 1984: The vertical distribution of macro-insects migrating in the nocturnal boundary layer: a radar study. *Bound. Lay. Meteor.*, 353-374.

Drake, V. A. 1985: Radar observations of moths migrating in a nocturnal low-level jet. *Ecol. Entomol.*, 259-265.

Drake V. A., and D. Reynolds, 2012: *Radar Entomology. Observing Insect Flight and Migration.* CABI, 489 pp.

Dual-Polarization Radar Principles and Systems Operations. 2018: Retrieved from Warning Decision Training Branch Web site: https://training.weather.gov/wdtd/courses/dualpol/documents/DualPolRadarPrinciples.pdf

Eastwood, E. 1967: *Radar Ornithology.* Methuen and Co., Ltd. 257 pp.

Federal Aviation Administration. 2016: *Wildlife strikes to Civil Aircraft in the United States 1990 - 2015, Report of the Associate Administration or Airports.* National Wildlife Strike Database Serial Report Number 22.

Friend, A. 1939: Continous cetermination of air-mass boundaries by radio. *Bull. Amer. Met. Soc*, 202-205.

Gauthreaux, S., and Belser, C. 1998: Display of bird movements on the WSR-88D: patterns and quantification. *Wea. and Forecasting.*, 453-464.

Gauthreaux, S., Mizrahi, D., and Belser, C. 1998b: Bird migration and bias of WSR-88D wind estimates. *Wea. and Forecasting.*, 465-481.

Geerts, B., and Miao, Q. 2005: Airborne Radar Observations of the Flight Behaviour of Small Insects in the Atmospheric Convective Boundary Layer. *Environmental Entomology*, 361-377.

Gossard, E., and Strauch, R. 1983: Radar Observations of Clear Air and Clouds. *Elsevier*, 280 pp.

Gourlery, J. J., Tabary, P., and Parent du Chatelet, J. 2006: A Fuzzy Logic Algorithm for the Separation of Precipitating from Nonprecipitating Echoes Using Polarimetric Radar Observations. *J. Atmos. Oceanic Technol.,***23**, 1340-1356.

Hardy, K., and Glover, K. 1966: 24 hour history of radar angel activity at three wavelengths. *Twelfth Conference on Radar Meteorology.* Norman, Oklahoma.

Hardy, K., and Katz, I. 1969: Probing the atmosphere with high power, high resolution radars. *Proceedings of the IEEE*, 468-480.

Jiang, Yu., Q. Xu, P. Zhang, K. Nai, and L. Liu,2013: Using WSR-88D polarimetric data to identify bird contaminated Doppler velocities. Advances in Meteorol.,Article 769275, 13 pp.

Jungbluth, K., Belles, J., and Schumacher, M. 1995: Velocity contamination of WSR-88D and wind profiling data due to migrating birds. *Preprints 27th Conference on Radar Meteorology*.

Keenan, T. D. 2003: Hydrometeor classification with a C-band polarimetric radar. *Aust. Meteor. Mag.*, 23-31.

Krause, J. M. 2016: A Simple Algorithm to Discriminate between Meteorological and Nonmeteorological Radar Echoes. *J. Atmos. Oceanic Technol.*, **33**, 1875-1885.

Kropfli, R. A. 1986: Single Doppler radar measurements of turbulence profiles in the convective boundary layer. *J. Atmos. Ocean. Tech.*, 305-314.

Kropfli, R., Katz, I., Konrad, T., and Dobson, E. 1968: Simultaneous radar reflectivity measurements and refractive index spectra in the clear atmosphere. *Radio Sci.*, 991-994.

Kumjian, M. R. 2013: Principles and applications of dual-polarization weather radar. Part I: Description of the polarimetric radar variables. *J. Operational Meteor.* **1** (20), 243–264.

Lane, J., and Meadows, R. 1963: Simultaneous radar and refractometer soudings of the troposphere. *Nature*, 35-36.

Lim, S., Chandrasekar, V., and Bringi, V. 2005: Hydrometeor classification system using dual-polarization radar measurements: Model improvement and in situ verification. *IEEE Trans. Geosci. Remote Sens.*, 792-801.

Liu, H., and Chandrasekar, V. 2000: Classification of Hydrometeors based on polarimetric radar measurements: Development of fuzzy logic and neuro-fuzzy systems and in situ verification. *J. Atmos. Oceanic Technol.*, 140-164.

Martin, W. 2003: *Measurements and Modelling of the Great Plains low-level jet.* Oklahoma: University of Oklahoma Graduate College.

Martin, W. and A. Shapiro, 2007: Discrimination of Bird and Insect Radar Echoes in Clear Air Using High-Resolution Radars, *J. Atmos. Oceanic Technol.*,24, 1215-1230.

Marzano, F., Scaranari, D., Montopoli, M., and Vulpiani, G. 2008: Supervised classification and estimation of hydrometeors from C-band dual-polarized radars: A Bayesian approach. *IEEE Trans. Geosci. Remote Sens.*, 85-98.

Melnikov, V. M., R. R. Lee, N. J. Langlieb, 2012: Resonance effects within S-band in echoes from birds. *IEEE Geosci. Remote Sens. Letters.* **9**, 413-416.

Melnikov, V. M., R. J. Doviak, D. S. Zrnic, D. J. Stensrud, 2011: Mapping Bragg scatter with a polarimetric WSR-88D, *J. Atmos. Oceanic Technol.,* **28**, pp. 1273-1285.

Melnikov, V.M., D.S. Zrnic, R.M. Rabin, and P. Zhang, 2008: Radar polarimetric signatures of fire plumes in Oklahoma. *Geophys. Res. Lett.*, **35**, L14815, doi:10.1029/2008GL034311.

Melnikov, V. M., D. S. Zrnic, R. M. Rabin, 2009: Polarimetric radar properties of smoke plumes: A model. Journal of Geophysical Research - D: Atmospheres, 114, doi:10.1029/2009JD012647.

Melnikov, V. M., R. J. Doviak, D. S. Zrnić, D. J. Stensrud, 2013: Structures of Bragg Scatter Observed with the Polarimetric WSR-88D. *J. Atmos. Oceanic Technol.*, **30**, 1253–1258.

Melnikov, V., and D. Zrnic, 2017: Observations of convective thermals with weather radar. *J. Atmos. Oceanic Technol.*, 34, 1585-1590.

Melnikov, V.M., M. Istok, and J.K. Westbrook, 2015: Asymmetric radar echo patterns from insects. *J. Atmos. Oceanic Technol.,***32**, 659-674.

Miller, P., Barth, M., Smart, J., and Benjamin, L. 1997: The extent of bird contamination in the hourly winds measured by the NOAA profiler network: results before and after implementation of the new bird contamination quality control check. *Preprints, 1st Symposium in Integrated Observing Systems*, pp. 138-44. Long Beach, CA.

NOAA's National Weather Service Radar Operations Center. (n.d.). Retrieved from https://www.roc.noaa.gov/WSR88D/Maps.aspx

Nohara, T.J., R. C. Beason, and P. Weber, 2011: Using radar cross-section to enhance situational awareness tools for airport avian radars, *Human-Wildlife Interact.*, **5**, no. 2

O'Bannon, T. 1995: Anomalous WSR-88D wind profiles - migrating birds? *Preprints, 21st Conference on Radar Meteorology*.

Park, H., Ryzhkov, A. V., S., Z. D., and K., K. 2007: Optimization of the Matrix of Weights in the Polarimetric algorithm for classification of radar echoes. *33rd Conf. on Radar Meteorology*. Cairns, QLD, Australia: Amer. Meteor. Soc.

Park, H., Ryzhkov, A. V., Zrnic, D. S., and Kim, K. 2008: The Hydrometeor Classification Algorithm for the Polarimetric WSR-88D: Description and Application to an MCS. *Weather and Forecasting*.

Patterson, T. 2016, September 12. *CNN*. Retrieved from CNN website: https://www.cnn.com/2016/09/09/us/sully-sullenberger-miracle-hudson-bird-strike-prevention/index.html

Radar Operations Center. (n.d.). Retrieved from NOAA's National Weather Service Radar Operations Center: https://www.roc.noaa.gov/WSR88D/Engineering/NEXRADTechInfo.aspx)

Riley, J. 1975: Collective orientation in night-flying insects. *Nature*, 113-114.

Schuur, T. J., Ryzhkov, A. V., and Heinselman, P. L. 2003: *Observations and classifications of echoes with the polarimetric WSR-88D radar.* Norman, OK: NOAA/National Severe Storms Laboratory Report.

Seidenman, P., and Spanovich, D. 2016: *How Bird Strikes Impact Engines*. http://aviationweek.com/author/paul-seidenman-amp-david-j-spanovich

Silverman, B. W. 1986: Density Estimation for Statistics and Data Analysis. *Monographs on Statistics and Applied Probability*.

Stepanian, P., Horton, K., Melnikov, V., Zrnic, D., and Gauthreaux Jr, S. 2016: Dual polarization radar products for biological applications. *Ecosphere*. 7(11) Article e01539.

Straka, J. M. 1996: Hydrometeor fields in a supercell storm as deduced from dual-polarization radar. *Preprints, 18th Conf. on Severe Local Storms* . 551-554). San Francisco, CA: Am. Meteor. Soc.

Straka, J., and Zrnic, D. 1993: An algorithm to deduce hydrometeor types and contents from multiparameter radar data. *Preprints, 26th Conf. on Radar Meteorology*, pp. 513-516. Norman, OK: Amer. Meteor. Soc.

U.S. Department of Commerce; National Oceanic and Atmospheric Administration. 2016: *Federal Meteorology Handbook No. 11: WSR-88D Meteorological Observations. Part A System Concepts, Responsibilities and Procedures.* Washington, DC.

U.S. Federal Aviation Administration, 2010: Airport Avian Radar Systems - Advisory Circular 150/5220-25.

van de Kamp, D., Ralph, F., Barth, M., Miller, P., Smart, J., and Benjamin, L. 1997: The new bird contamination quality control check applied to hourly winds from NOAA's profiler network. *Preprints, 28th Conference on Radar Meteorology.* Austin, Texas: Amer. Meteor. Soc.

Vivekanandan, J., Zrnic, D. S., Ellis, S., Oye, D., Ryzhkov, A., and Straka, J. 1999: Cloud microphysics retrieval using S-band dual-polariation radar measurements. *Bull. Amer. Meteor. Soc.*, 381-388.

Wikipedia. 2009, June 20. Retrieved from https://en.wikipedia.org/wiki/Bird_strike#/media/File:Jet_engine_damaged_by_bird_strike.jpg

Wilczak, J. M., Strauch, R. G., Ralph, F. M., Weber, B. L., Merrit, D. A., Jordan, J. R., . . . Riddle, A. C. 1995: Contamination of wind profiler data by migrating birds: characteristics of corrupted data and potential solutions. *J. Atmos. Oceanic Technol.,*, 449-67.

Wilson, J., Weckwerth, T., Vivekanandan, J., Wakimoto, R., and Russel, R. 1994: Boundary layer clear-air radar echoes: origins of echoes and accurracy of derived winds. *J. Atmos. and Ocean. Tech*, 1184-1206.

Zehnder, G. 2014, March 12: *Extension*. Retrieved from Extension: http://articles.extension.org/pages/19198/overview-of-monitoring-and-identification-techniques-for-insect-pests

Zrnic, D., and Ryzhkov, A. 1998: Observations of insects and birds with a polarimetric radar. *IEEE Trans. on Geos. and Remote Sensing*.

Zrnic, D., and Ryzhkov, A. 1999: Polarimetry for weather surveillance radars. *Bull. Amer. Met. Soc.*, **80,** 389-406.

Zrnic, D., Ryzhkov, A., Straka, J. M., Liu, Y., and Vivekanandan. 2001: Testing a procedure for the automatic classification of hydrometeor types. *J. Atmos. Oceanic Technol.*, 892-913.